PHASE CHANGE MATERIALS FOR SOLAR THERMAL ENERGY STORAGE

by

Paul M. Allred

Submitted in partial fulfillment of the
requirements for the degree of
Master of Science

at

Dalhousie University
Halifax, Nova Scotia
March 2014

To dæmons

spirits of creativity

Table of Contents

List of Tables

List of Figures

Abstract

Phase change materials (PCMs) are a viable option for compact thermal energy storage. Effective designs using PCMs require accurate knowledge of the thermal and physical properties, but for many PCMs these are not well known, and when known the knowledge is sometimes contradictory. Therefore, physical characteristics of several promising PCMs ($K_3PO_4 \cdot 7H_2O$, $FeCl_3 \cdot 6H_2O$, $Mn(NO_3)_2 \cdot 4H_2O$) were determined. In addition, a life cycle assessment (LCA) of dodecanoic acid in a solar thermal energy storage system was carried out to determine the environmental impact for energy storage. This LCA showed that dodecanoic acid in a solar energy system would save energy and facilitate CO_2 reductions. However, the economic cost is high and is unlikely to be implemented without incentives. Finally an experimental testbed for a solar thermal system utilizing dodecanoic acid was built. Preliminary measurements demonstrated the utility of this system.

List of Symbols and Abbreviations Used

Symbols

a Lattice parameter of monoclinic crystal system

a Absorptivity

A Area or surface area

Subscripts

$_{c}$ Effective convective surface area of tube

$_{collector}$ Area of solar collector

$_{pipe}$ Cross-sectional area of pipe

b Lattice parameter of monoclinic crystal system

Bi Biot number

c Lattice parameter of monoclinic crystal system

C Specific heat capacity at constant pressure

Subscripts

$_{p}$ at constant pressure

$_{p,htf}$ of heat transfer fluid at constant pressure

$_{p,l}$ of liquid material at constant pressure

$_{p,s}$ of solid material at constant pressure

$_{p,t}$ of tube at constant pressure

E Energy

Subscripts

$_{collector}$ absorbed by collector

$_{PCM}$ absorbed by phase change material

h Natural convective heat transfer coefficient of air

H Enthalpy

I Solar irradiance

m Mass

Subscripts

$_{p}$ of phase change material

$_{t}$ of tube

$_{w}$ of standard(water)

Q Heat

R Radius

t Time

T Temperature

Subscripts

$_{0}$ of material at start of experiment

$_{i}$ of inflection, or point at which solidification is complete

$_{inlet}$ of inlet

$_{m}$ of Melting

$_{outlet}$ of outlet

$_{r}$ of material at end of experiment

$_{s}$ of onset of solidification

$_{\infty,a}$ of ambient at end of experiment

v Velocity

β Lattice parameter of monoclinic crystal system

Δ Change or in parameter, *e.g.* temperature or enthalpy

Δh_p enthapy change of material over a small temperature range

Δ_{fus}H Enthalpy of fusion

ΔH_m Enthalpy of fusion (melting)

κ Thermal conductivity

ρ Density

ρ_{htf} Density of heat transfer fluid

Abbreviations

PCM Phase change material

DSC Differential scanning calorimetry or calorimeter

TGA Thermogravimetric analysis

LCA Life cycle assessment

FFB Fresh fruit bunch

POME Palm oil mill effluent

CPKO Crude palm kernel oil

CPO Crude palm oil

EFB Empty fruit bunch

NSCC Nova Scotia Community College

TES Thermal energy storage

DREAMS Dalhousie Research in Energy, Advanced Materials and Sustainability

Acknowledgements

Thank you very much Dr. Mary Anne White for supervising me during this work. Thank you to my supervisory committee, Dr. Dominic Groulx and Dr. Mark Obrovac I would like to specially thank Dr. Alain Joseph for his lab space and help in setting up the solar energy system at Nova Scotia Community College. I appreciate current and former group members for all of their help and time, listed here in alphabetical order: Adam Bent, Alex Bourque, Dr. Ran Chen, Jacy Conrad, Louis Desgrosseilliers, Michel Johnson, Dr. Samer Kahwaji, Dr. Kimberly Miller, John Niven, John Noël, Jan Pöhls, Dr. Andrew Ritchie, Carl Romao, and Dr. Catherine Whitman. Babak Farsi, and Phil Mackenzie of Scotian WindFields Inc. supplied the solar thermal panel used in this thesis and for that I thank them. Finally, I would like to give thanks to the NSERC CREATE program, DREAMS for financial support.

Chapter 1

Introduction

Phase change materials provide a viable option for effective and compact thermal energy storage. In Chapter 1, the concepts of phase change materials (PCMs) and thermal energy storage are discussed. Chapter 2 summarizes the materials and methods used throughout the rest of the thesis. Chapter 3 discusses the characterization of several phase change materials. Chapter 4 presents a life cycle assessment of a specific phase change material, dodecanoic acid, and a solar thermal energy storage system utilizing it. Chapter 5 presents a case study of the thermal heat transfer characteristics of an actual solar thermal energy system utilizing dodecanoic acid. The final chapter, 6, is a concluding chapter summarizing the salient points of the thesis.

1.1 Thermal Energy Storage

There is an energy crisis and the world is faced with global warming and climate change. The Intergovernmental Panel on Climate Change Fifth Assessment Summary for Policymakers reports an unequivocal warming of the ocean and the atmosphere and concludes that it is "extremely likely" that human influence has been the dominant cause of the warming [1]. Because the burning of fossil fuels for energy has been the chief factor in this human influence, renewable energy resources are necessary to help solve our dependency on fossil fuels. However, most renewable energy sources, such as wind, solar, and tidal power, are intermittent and are not sufficient to provide for the entirety of humanity's energy consumption [1]. Clearly, it is necessary to use energy more wisely. What is often overlooked, however, is the importance of finding and using alternative methods to store energy. Often when people think of energy usage, they focus primarily on electricity, and the role that space and water heating has in energy consumption is overlooked. About 20% of all energy used in Canada is used in either heating water or air [2]. Heating also accounts for 70% of residential

energy use and about 60% of institutional or commercial energy use [2].

Heat is normally waste energy. Usually it is produced as a byproduct or inefficiency of some other energy process. However, there are many circumstances when heat is needed. For example, heat is needed to provide thermal comfort for people in their homes during cold seasons. Hot water is also required for cooking and cleaning. But other conditions may call for the reduction of heat. Many foods need to be cooled to be kept fresh. Blood or organs for medical transplants are also kept on ice to preserve them [3]. How best does one go about producing, storing, utilizing and moderating heat?

For eons people have been aware of the power of using materials to store heat, especially from the sun, to make living spaces thermally comfortable. Structures have been built with thick clay, stone, mud, or brick walls for about as long as people have been building houses. These materials are considered to have a high "thermal mass," *i.e.* they can store a large amount of heat [4]. In hot summer months during the day, the sun heats the walls, and the interior remains cool. If the temperature decreases at night the walls then transfer the heat they have absorbed back into the living space, keeping the inside of the building relatively warm. During the winter months the thick walls are useful for the same reason. Although the sun is not always intense enough to provide sufficient heat to warm the building, other heat sources such as a wood-burning fireplace will serve essentially the same function as the sun. In this case, although the walls will make it more difficult to get the room warmer initially, once the walls are warm, the room will retain heat even after the fire has gone out.

The method of storing heat by causing an increase of temperature in an object is known as sensible heat. Because the energy is stored by increasing the temperature of the object, the amount of heat that can be stored is proportional to the specific heat capacity, C_p, of the material. Mathematically this is expressed as $Q = mC_p\Delta T$, where Q is the heat stored, m is the mass, and ΔT is the change in temperature. For most materials C_p is relatively small, (typically less than 2 kJ kg^{-1}) therefore to store an appreciable amount of heat, m or ΔT or both must be large. In the case of the walls given above, ΔT is mostly fixed by the thermal comfort requirements so the mass of the walls must be large, hence the walls must be thick. Usually the amount

of heat stored is expressed independent of mass as,

$$\Delta H = \int_{T_1}^{T_2} C_p(T)\ dT, \tag{1.1}$$

where ΔH is the enthalpy change in kJ kg^{-1}, and $C_p(T)$ is the temperature dependent specific heat capacity, so that an energy storage density can be estimated. The constant pressure heat capacity, C_p, is used here because the pressure remains relatively constant in almost all normal applications of thermal storage materials. In the next section another form of heat storage, known as latent heat, is discussed. This is the form that PCMs exploit to exhibit high thermal energy density.

1.2 Phase Change Materials

Phase change materials are a class of materials that use a phase transition to store energy. A phase transition occurs when a material changes from one state of matter to another without changing its chemical composition, for example from liquid to solid or from solid to gas. Although transitions involving gas have very large enthalpies of transition, containing a large mass of gas is very difficult, requiring expensive and potentially dangerous pressure vessels. Therefore almost all practical PCMs will have solid-liquid transitions [5]. There are some materials that exhibit solid-solid transitions; these have a much lower enthalpy of transition. Solid-solid transitions involve a change in the crystal structure of the material, for example iron changes from body-centered cubic to face-centered cubic at 1185 K [6]. Solid-solid transitions are advantageous from the perspective that they do not require containment the way solid-liquid materials do [7, 8].

It takes energy to break the bonds present in a crystalline solid, and this energy, often called latent heat, can be used to store heat in a material. The amount of heat a latent heat storage material can store over a temperature range, T_1 to T_2 which includes melting, is given by

$$\Delta H = \int_{T_1}^{T_m} C_{p,s}(T)dT + \Delta H_m + \int_{T_m}^{T_2} C_{p,l}(T)\ dT, \tag{1.2}$$

where T_m is the melting temperature, $C_{p,s}$ and $C_{p,l}$ are the solid and liquid heat capacities respectively, and ΔH_m is the enthalpy of transition [5, 9]. Note that Equation

1.2 is nearly identical to Equation 1.1, except that there is an additional term for the enthalpy of transition.

1.2.1 PCM Selection Criteria

A good phase change material must meet certain criteria and possess certain material characteristics. These have been listed in a number of reviews by various authors and they are summarized below [3, 5, 9, 10, 11, 12].

Many thermodynamic criteria must be met in order for a PCM to be considered a viable PCM. The material should have a large enthalpy of transition, *i.e.* latent heat, otherwise known as ΔH_m. The purpose of a PCM is to store heat, so the more heat stored the better the material. However, it is important to consider if the specific or volumetric latent heat is more important for the application. Typically, space is the limiting factor, so more often the volumetric latent heat should be considered. Since density changes on phase change and as a function of temperature, the lowest density in the operating temperature range is used to calculate volumetric latent heat; at the lowest density the material takes up the most volume, which sets the size of the PCM. The material should have a high heat capacity in both the liquid and solid phase. As few applications use only the latent heat of a material, having a high heat capacity allows for more thermal storage in the sensible regime. For the application desired, the PCM should have an appropriate melting point, T_m. If the material does not have a melting point at the application temperature, the PCM is no better than a sensible heat storage material. The material should have a congruent melting point and a small melting range. Impure materials or incongruently melting materials can have wide melting temperature ranges which complicate matters when thermally cycling. For example, stratification may occur with heavier portions settling to the bottom. A high thermal conductivity, κ, is also needed. Materials with high thermal conductivity allow quick heating and cooling to occur for good power input and output.

PCMs have a few kinetic criteria that must be met as well. They should exhibit a small amount of supercooling, which occurs when a material fails to crystallize at its melting temperature. Most materials supercool a few degrees but some PCMs can exhibit supercooling on the order of 80 K. The crystal growth rate of the material must also be high. When the materials begin to solidify, if the rate is too slow, it

is difficult to take energy out of the system. Crystal growth rate is a complicated problem that is related to a number of material properties, from viscosity to thermal conductivity. Essentially, the growth rate is dependent on the heat and mass transfer properties of the material [5].

The chemical criteria are mostly related to safety and containment issues. The PCM must have long term chemical stability, and be able to withstand thousands of repeated freeze-thaw cycles without degrading significantly. To minimize leakage, the material should be non-corrosive, as corrosive materials can eat away at containers. Chemical reactions between the container and PCM should be kept at a minimum. Little or no leakage should occur during the life of the PCM, but in the case that there is an accident, the PCM should be non-flammable and non-toxic, neither deadly nor harmful.

Finally, there are a few economic requirements that must be considered. Since most applications require large amounts of PCM, the cost of the PCM must be low. Of course, there is some uncertainty here because of the fluctuation of market prices and the possibility that alternative manufacturing methods might be developed for the material should the demand be increased. At the very least the material should not contain any rare elements, since this would unnecessarily increase the cost. The material should also be environmentally friendly. If the goal of using PCMs is to help reduce greenhouse gas emissions and save energy, then the material should not be excessively difficult to produce or cause undue environmental damage in its production.

No single material can possibly fulfill all of these stringent requirements, and engineering solutions must be made to accommodate any shortfalls [9].

1.2.2 PCM Categories

There are many different types of potential phase change materials; any material with a melting point is a potential candidate. Largely through the work of Lane a few broad categories of potential PCMs were delineated [13, 14]. Lane sorted through tens of thousands of materials to find candidates that could be good PCMs. There are two main categories that naturally form, inorganic and organic, which are broken up into several major subcategories. In the inorganic group there are metals, salt hydrates, water, and salts. Organic PCMs include: paraffin waxes, which are long

chain hydrocarbons; fatty acids and esters; sugar alcohols; and other miscellaneous organic compounds. Additionally, there are mixtures of the above categories both in eutectic and non-eutectic mixtures. Each broad category has some advantages and disadvantages which are discussed below.

Metals

Metallic PCMs have extremely high thermal storage density and thermal conductivity. However, they are expensive and tend to have high melting points. Although there are low melting point eutectics, they are dense (which can be advantageous or disadvantageous depending on the application), costly and often contain lead, which is harmful to life. The liquid metals are often corrosive to metal containers but can be stored in ceramic, glass, or polymer containers. Properly stored metals have extremely good stability and cycle life, and experience almost no supercooling [9].

Salt Hydrates

Salt hydrates are a special class of PCM. Strictly speaking they do not usually exhibit melting like a metal or other pure substance does. Upon heating the salt hydrate loses its water of hydration and the salt dissolves in the liberated water [5]. These processes happen simultaneously, so when a salt hydrate is heated it appears as if it is melting. The process of water leaving the salt crystal is endothermic much like melting is, thus it also stores heat in much the same way a normal melting material can. However, the dissolution of the salt in water is slightly exothermic, which decreases the amount of heat that can be stored. The heat of dissolution is much smaller than the heat of decomposition, so the net effect is strongly endothermic [5].

In general, salt hydrates have relatively large heats of fusion. Their thermal conductivities are moderate—low compared to metals, but high compared to most organics. Salt hydrates are the cheapest class of materials, often costing less than one dollar per kilogram. Corrosion can be an issue with metallic containers, but polymers work quite well [15]. Cycle life is usually good with the exception of incongruently melting materials. The most notable incongruently melting salt hydrate is $Na_2SO_4 \cdot 10H_2O$, which had initial promise but without additives would quickly stratify and become almost useless as a heat storage material [16]. Supercooling is also a great concern with

many salt hydrates. Some, such as $Ca(NO_3)_2{\cdot}4H_2O$, have been known to supercool in excess of 80 K even at slow cooling rates to the point where they experience a glass transition [17]. There have been efforts to overcome this problem by using nucleation agents [5, 16]. Salt hydrates also have a good range of melting temperatures for solar thermal applications, in the approximate range of 0 to 300 °C.

Water

Water is unique enough to deserve its own category. It has an extremely high heat capacity and heat of fusion. Whereas most materials have a heat capacity of about 1-2 kJ kg^{-1}, water has a heat capacity of 4.18 kJ kg^{-1}. Heat of fusion is roughly proportional to melting point but water has a heat of fusion about triple (335 kJ kg^{-1}, 307 kJ L^{-1}) typical values for its melting point [18]. Solid water has a relatively low density (0.9167 kg L^{-1} [6]), which means that it takes up more volume than many other phase change materials. Water is also the cheapest phase change material, costing mere pennies per kg. Its cycle life is very good and supercooling is not a problem unless the water is extremely pure. When it is properly stored, corrosion is not an issue and its thermal conductivity is adequate for many applications, although water experiences large expansion upon freezing that can cause some issues during storage. The most significant limitation for its broad use as a PCM is that the melting point is essentially fixed. Although some additives can be used to lower the freezing point, there is no feasible way to make it much higher. Still, water finds many applications as a PCM, particularly in the air conditioning industry. For example, some large buildings use cheap nighttime electricity to freeze quantities of water and then during the day use the ice for air conditioning [3].

Anhydrous salts

Anhydrous salts are also potential phase change materials. These have generally good properties, *i.e.* a high enthalpy of fusion, heat capacity and thermal conductivity, and as such are often used as heat transfer fluids for concentrated solar thermal energy. The high salt melting temperatures (*ca.* 300 to 800 ℃), and the corrosive nature of molten salts mean that significant precautions must be taken to safely use salts as a PCM [3, 18]. Salts are generally inexpensive, unless a comparatively rare element

such as cesium is used.

Paraffin waxes

Paraffin waxes are mixtures of long saturated hydrocarbon chains, typically greater than ten carbons, and they have many desirable properties. Although their heat of fusion is lower than most other materials, it is still high enough to be of use in many applications. They have a good cycle life and low supercooling [3]. The paraffin wax thermal conductivity is the lowest (on the order of 0.15 W m^{-1} K^{-1}) of any PCM class. As far as cost goes, they are relatively expensive, though not prohibitively so, even for large scale applications. Although, as petroleum byproducts they may not be environmentally friendly to extract, it can be argued that at least they are not being burned as fuel, releasing more greenhouse gases. They have a range of melting temperatures from 10 to 200 ℃ with many potential applications.

Fatty acids and esters

Fatty acids are similar to paraffin waxes in that they are long hydrocarbon chains and as such they have similar properties. However, they contain an acid group. Fatty esters are fatty acids that have undergone an esterification to connect an alkyl group. This gives them slightly different properties than the fatty acids, but they are still similar enough to group them together. In general, the esters are less corrosive and more sluggish to crystallize than their acid cousins [9]. A few examples of fatty acids and esters are shown in Figures 1.1 and 1.2 respectively.

Fatty acids share most of the advantages and disadvantages of paraffins. But because they can be plant-derived fatty acids are more environmentally friendly than paraffins [9, 19, 20]. However, because they are acids, there are also a few concerns with storage and encapsulation, but these can be overcome using appropriate materials, such as stainless steel [21]. At temperatures around 150 to 200℃ they tend to decompose so their applications are limited to lower temperature ranges [9].

1.2.3 Phase Change Material Characterization and Selection

As mentioned above, a great deal of work has been done to identify many materials that would function effectively as PCMs. Usually for each material studied, only the

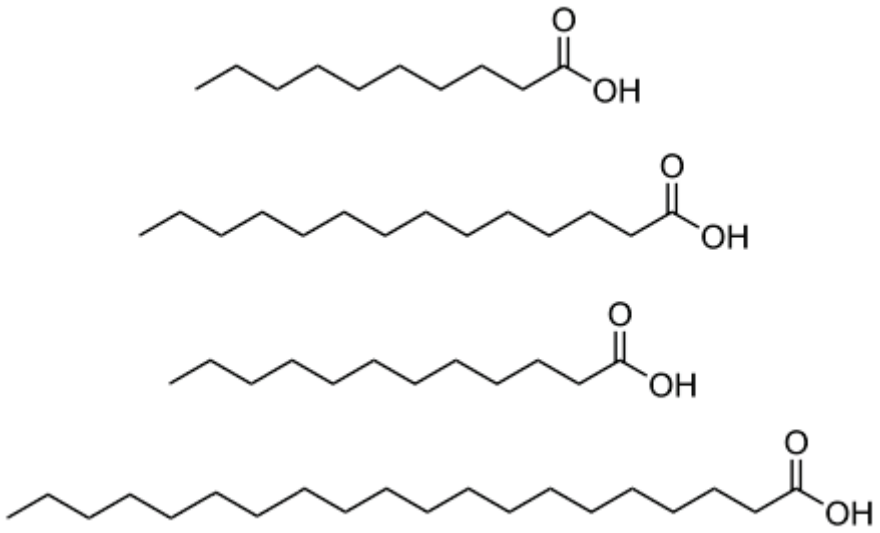

Figure 1.1: Examples of fatty acids. From top to bottom they are decanoic acid, tetradecanoic acid, dodecanoic acid, and eicosanoic acid.

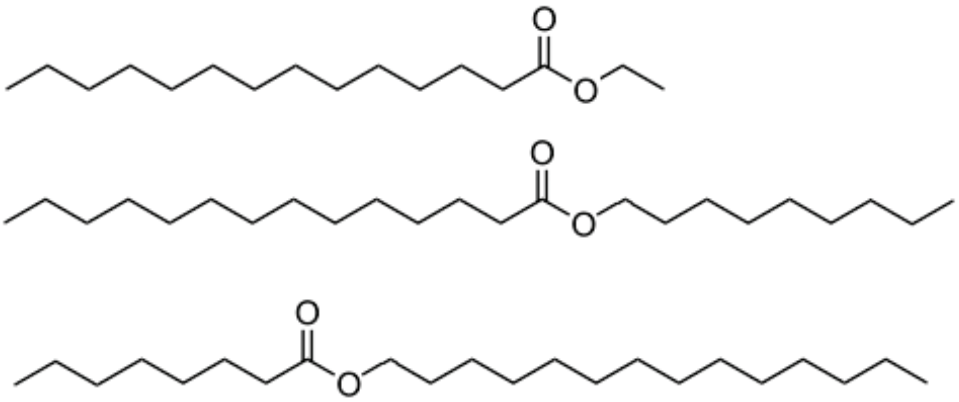

Figure 1.2: Examples of fatty esters. Fatty esters can have either long or short groups on either side. From top to bottom the examples shown are ethyl tetradecanoate, nonyl tetradecanoate, and tetradecyl octanoate.

enthalpy of transition and the melting point are reported, with some relative ranking as to its potential quality as a PCM [10, 13, 14, 22]. These initial results have been repeated in numerous reviews, often including and propagating errors and typos [3, 9, 11, 12] causing a deal of confusion to a newcomer to the field. However, knowledge of many other properties of phase change materials is necessary for adequate engineering and design in all applications. For example, the temperature dependent thermal conductivity of the material is needed to design heat transfer fin spacing for a heat exchanger [11], and the heat capacity must be known to design for the sensible heat portion of the thermal energy storage [23].

In order to meet the challenges created by these inadequacies a list was compiled based on an extensive literature search. This list brings together as many material properties as possible for the materials included. This way, once a material is selected as a candidate PCM, it would be clear which material properties still needed to be determined accurately. The materials included in the list were materials already determined to have some potential as a PCM in the PCM literature, but instead of just using the value given in the review, effort was taken to find a primary source or at least a reliable secondary source such as National Institute of Standards and Technology Chemistry WebBook [24], the CRC Handbook of Chemistry and Physics [6] or Yaws' Handbook of Chemical Properties [25]. Over 550 materials, citing nearly one hundred sources, were cataloged listing the characteristics, heat of fusion, melting point, thermal conductivity of liquid and solid, density of liquid and solid, heat capacity of liquid and solid, melting behavior, safety, and approximate commodity cost. There is also an indication of the temperature at which a specific property was recorded, or if temperature dependence is available in the source. While this list is too comprehensive to include here, a snippet of its contents is shown in Figure 1.3.

The overarching goals of this thesis work were to establish materials and methods that advance research in the field of PCMs for solar energy storage. The extensive compilation of PCMs described above revealed several salt hydrates that had potential. These were characterized experimentally because few salt hydrates are being used for practical applications but they have many desirable properties. Results of these experiments are presented in Chapter 3.

Once a material has been determined to have the necessary characteristics for

PCM	Type	Melting Point (°C)	Latent Heat (kJ/kg)	Latent Heat (kJ/L)	Thermal Conductivity (solid)($Wm^{-1}K^{-1}$)	Thermal Conductivity (liquid) ($Wm^{-1}K^{-1}$)	Heat Capacity (solid) (kJ/kgK)	Heat Capacity (liquid) (kJ/kgK)	Density (solid)(kg/L)	Density (liquid)(kg/L)	Toxicity & Safety
Zinc Nitrate Hexahydrate	Salt Hydrate	36	147	269		0.464	1.34	2.26	2	1.828	Eye Irritant; do not ingest/inhale.
ı hydrogen phosphate dibasic dodeca	Salt Hydrate	36	280	403	0.51	0.48	1.7	1.95	1.522	1.44	
Capric acid	Organic, fatty acid	36	152								
Zinc Nitrate Hexahydrate	Salt Hydrate	36.1	134	245		0.469	1.34	2.26	1.937	1.828	Eye Irritant; do not ingest/inhale.
Ethylene carbonate	Organic	36.34	151.0	199					1.321		
Zinc Nitrate Hexahydrate	Salt Hydrate	36.4	147	269		0.469	1.06	2.26	2.067	1.828	Eye Irritant; do not ingest/inhale.
Zinc Nitrate Hexahydrate	Salt Hydrate	36.4	147	269		0.469	1.34	2.26	1.937	1.828	Eye Irritant; do not ingest/inhale.
n-Eicosane	Organic, Paraffin	36.6	247.3	195				2.35	0.789		Eye Irritant; do not ingest/inhale. HARMFUL
Ferric Chloride Hexahydrate	Salt Hydrate	37	223	368			1.02		1.82	1.649	
Manganese Nitrate Tetrahydrate	Salt Hydrate	37.1	115	245			1.04		2.13		
nonadecyl acetate	Organic, ester	37.6	166.94			0.1619	1.8206	2.0926	0.8428	0.843	
methyl stearate	Organic, ester	37.78	64.43			0.1688	1.7996	1.9774	0.8498	0.8503	
Titanium tetrabromide	Inorganic	38	23.45	61					2.6		Corrosive, lachrymator
1-Tetradecanol	Organic	38	205								
Sodium sulfate decahydrate	Salt hydrate	39	180	263	0.3	0.15	2.0	2.0	1.460		
Calcium Bromide Hexahydrate	Salt Hydrate	39	115	225			0.812		2.194	1.956	Eye Irritant; do not ingest/inhale.
Camphenilone	Organic	39	205								
eicosyl acetate	Organic, ester	40	167.66			0.1618	1.8385	2.1942	0.842	0.845	
ium Hydrogen Phosphate Dodecahyd	Salt Hydrate	40	279	402	0.51	0.48	1.7	1.95	1.52	1.44	
Medicinal paraffin	Organic, paraffin	40	146	121	0.5				0.830		
Docasyl bromide (1-bromodocosane)	Organic	40	201	209					1.04		Eye Irritant; do not ingest/inhale.

Figure 1.3: A snippet of a much larger sortable spreadsheet containing information on characteristics, heat of fusion, melting point, thermal conductivity of liquid and solid, density of liquid and solid, heat capacity of liquid and solid, melting behavior, safety, and approximate commodity cost for about 550 potential phase change materials.

application as a PCM more research is still required. Specifically, when developing a material that will be used to save energy or prevent CO_2 emissions, the environmental impact of producing that material must be determined. Therefore, a life cycle assessment was carried out for a PCM, dodecanoic acid, that previously was established to have excellent potential for solar thermal energy storage applications. The life cycle analysis is presented in Chapter 4.

Finally, once the characteristics and feasibility of a PCM are determined, practical application and engineering of the PCM storage system must be carried out. To that end, a solar thermal storage system utilizing dodecanoic acid was constructed to function as a testbed for practical experiments to test how to best engineer a solar thermal PCM energy storage system. Preliminary measurements were taken to establish that it was an effective testbed. The results for this solar thermal storage test system are presented in Chapter 5.

Taken as a whole, the thesis work presented here represents the first steps in parallel efforts at each stage of PCM research and development.

Chapter 2

Materials and Methods

2.1 Phase Change Materials Used

The phase change materials selected for study were $FeCl_3{\cdot}6H_2O$ (Sigma-Aldrich, 99%), $Mn(NO_3)_2{\cdot}4H_2O$ (Alfa Aesar, 98%), and $K_3PO_4{\cdot}7H_2O$ (BDH, 98%) which were used as received for all experiments. These materials were selected because they fit many of the criteria outlined in the previous chapter and because there is a dearth of material properties for them in the literature. With a $\Delta_{fus}H$ of 223 kJ kg^{-1} (366 kJ L^{-1}),* $FeCl_3{\cdot}6H_2O$ has one of the highest heats of fusion of any salt hydrate and the melting point of 37 ℃ is well suited for many thermal energy storage applications [9]. $Mn(NO_3)_2{\cdot}4H_2O$ was selected because it is relatively cheap, known to not supercool extensively, and has a good melting point at 37.1 ℃. However, at 115 kJ kg^{-1} (245 kJ L^{-1})† its $\Delta_{fus}H$ is somewhat lower than desirable [9], but still higher than most fatty acids or paraffins. The melting point (45 ℃ [5]) of $K_3PO_4{\cdot}7H_2O$ was known, but not the $\Delta_{fus}H$. The anhydrous form (K_3PO_4) is a common food additive, which indicates it already is in relatively wide use. The solar thermal system described in Chapter 5 used dodecanoic acid (Alfa Aesar 98%), which has a melting point of 43.3 ℃ and a $\Delta_{fus}H$ of 184 kJ kg^{-1} (160 kJ L^{-1})‡ [26].

2.2 Differential Scanning Calorimetry

A TA instruments DSC Q200 was used to measure melting enthalpy changes and transition temperatures. A quick overview of how a differential scanning calorimeter (DSC) works is in order to fully understand the data presented. Inside the DSC there are two stages with independent heaters and thermometers in an isolated chamber. The sample is placed on one stage (inside of a sealed pan) and an empty pan or

*Calculated using liquid density measured in this thesis.
†Calculated using solid density [25].
‡Calculated using liquid density [25].

reference is placed on the other stage. Power is applied to both stages so as to keep them at identical temperatures. The temperature is gradually increased (or decreased) at some predetermined rate and the difference in power required to keep the stages at the same temperature is measured. For instance, during heating, if the sample were melting it would require considerably more power to match the temperature ramp rate than the reference would. By calibrating the DSC with a known sample with a well-defined transition temperature and enthalpy of fusion, it is possible to integrate under the power versus time curve to obtain transition enthalpy changes and onset temperatures for melting [27]. Reference materials for calibration are almost always metals, especially those that are readily available in high purities with well known melting points and heats of fusion. For example, indium, bismuth and zinc are commonly used calibration materials [27].

The DSC used in this study was calibrated using an indium standard ($T_m = 429.75$ K and $\Delta H = 3.81$ kJ/mol) [6]. All samples were sealed in Perkin-Elmer volatile sample aluminum DSC pans. The samples were placed in an isolated chamber with helium gas flowing at a constant rate of 25 mL min^{-1} through the chamber. Liquid nitrogen was used to cool the stages. Typical heating and cooling rates were 10 K min^{-1} for enthalpy measurement and 1 K min^{-1} for melting or freezing temperature measurements. There were usually three replicates measured for each sample, although for some there were as many as ten. The sample masses were usually around 10-20 mg.

2.3 Thermogravimetric Analysis

The amount of hydration of the salt hydrates was measured using thermogravimetric analysis (TGA) on a Netzsch TG 209F3. TGA is a method where mass is obtained as a function of temperature. The sample is placed in an open pan on a stage which serves both as a heater and a sensitive scale. The chamber is sealed and a gas is made to flow through the chamber at a fixed rate. As the sample is heated (or cooled in some cases) it may lose or gain mass through oxidation, decomposition, deposition, or evaporation. The scale measures the mass of the sample throughout the procedure as a function of temperature [27].

For this study TGA was used since the water component of salt hydrates is usually volatile at high temperatures; it is often possible to evaporate all of the water and

leave behind the salt components. This method allows for measurement of the degree of hydration of the salt hydrates.

For the TGA experiments performed in this study, the typical masses were about 50 mg. The temperature ramp rate was set to 10 K min^{-1} for all samples and argon gas was used during all measurements.

2.4 T-history

Günther *et al.* [28] highlight the issues that plague DSC when trying to measure the thermal properties of PCMs. The small sample size causes extreme supercooling that may not exist in bulk, because nucleation is a statistical phenomenon. With more material the probability that a seed crystal spontaneously forms increases. The high enthalpy and low thermal conductivity of most PCMs also causes difficulties during DSC measurements. Furthermore, almost no actual PCM applications use a pure material; additives are used to control melting point, prevent stratification, enhance thermal conductivity and promote nucleation. The small sample size used for DSC measurements does not allow these additives to be measured as well. Because of these issues, Zhang *et al.* [29] first proposed in 1999 a method for measuring the enthalpy of fusion and a few other pertinent properties of PCMs in bulk, which eliminates spurious effects due to small sample size (as in DSC) and allows for non-homogeneous samples to be measured. The method exposes tubes of PCM and a standard material to the same ambient atmosphere of still air. Then both samples have the same thermal history, which gives the method its name (T-history). By measuring the temperatures as a function of time it is possible to solve for liquid and solid heat capacities and for the melting enthalpy change. Examples of what typical T-history curves might look like for a PCM and the standard are shown in Figures 2.1 and 2.2, respectively.

Because the amount of heat transferred from the tubes both by radiation and by conduction is so low compared with the amount carried by natural convection, the temperature change of the sample over a fixed time prior to solidification can be written as,

$$(m_t C_{p,t} + m_p C_{p,l})(T_0 - T_s) = hA_c \int_0^{t_1} (T - T_{\infty,a})\, dt = hA_c A_1 \tag{2.1}$$

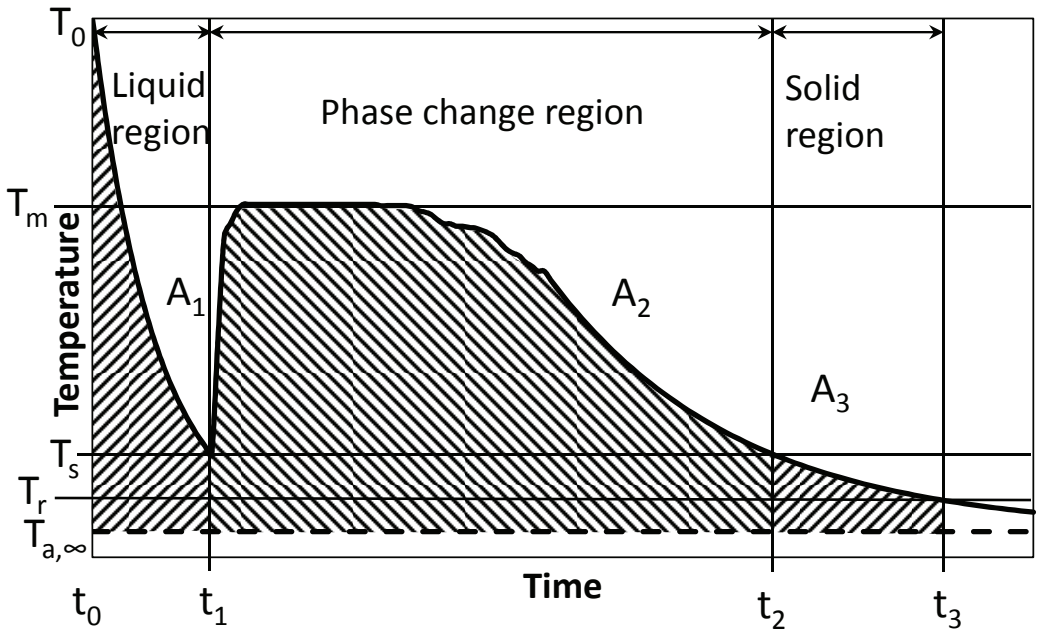

Figure 2.1: A typical T-history cooling curve of a PCM exhibiting supercooling. In A_1 only liquid is present. After t_1, in A_2, solidification has started and liquid and solid are present together. Between t_2 and t_3, in A_3, only solid remains and the material rapidly cools toward ambient. Note that supercooling results in $T_s \ll T_m$, where T_m is the melting point and T_s is the solidification temperature, and A_3 is therefore much smaller than it would be without supercooling.

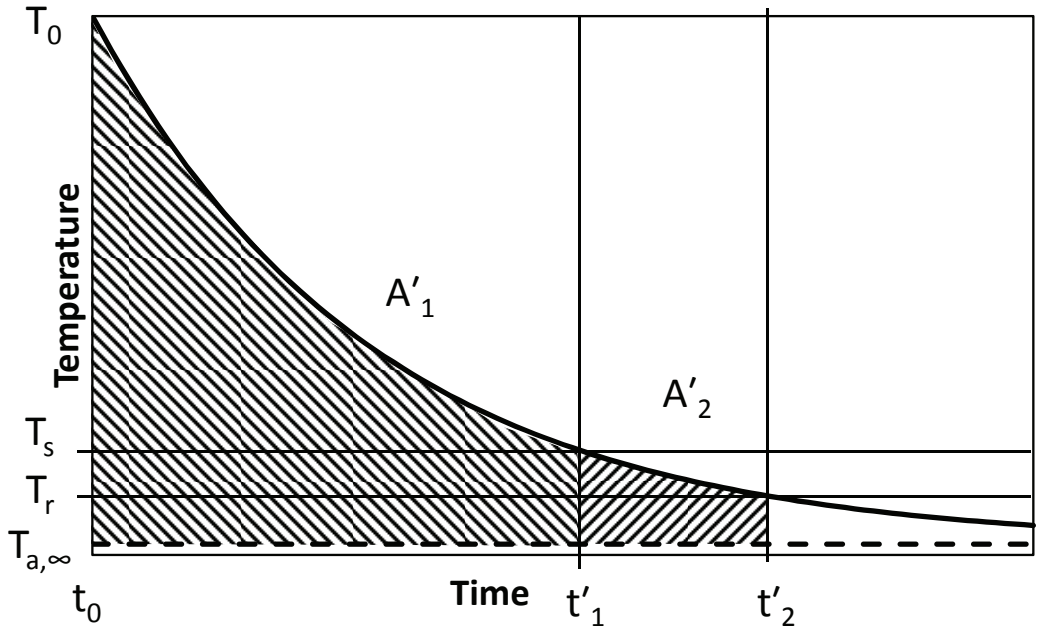

Figure 2.2: A typical T-history cooling curve for a standard material, such as water. Since there is no phase change in this temperature range the standard cools quickly toward ambient temperature.

where m_p and m_t are the masses of the PCM and the tube, $C_{p,t}$ and $C_{p,l}$ are the heat capacities of the tubes and liquid PCM respectively; T_0, T_s, and $T_{\infty,a}$ are the initial, solidification, and ambient temperatures; h is the natural convective heat transfer coefficient of air; t_1 is the onset time of solidification; A_1 is the area defined by the integral in Equation 2.1; and A_c is the convective surface area of the tube. The region of the phase transition is represented by

$$m_p \Delta H_m = hA_c \int_{t_1}^{t_2} (T - T_{\infty,a})\ dt = hA_c A_2 \tag{2.2}$$

where m_p is the mass of the PCM, ΔH_m is the melting enthalpy change, A_2 is the area defined by the integral in Equation 2.2, and t_2 is the time when solidification is complete. Finally, the last region where the solid cools to ambient temperature is expressed as

$$(m_t C_{p,t} + m_p C_{p,s})(T_s - T_r) = hA_c \int_{t_2}^{t_3} (T - T_{\infty,a})\ dt = hA_c A_3 \tag{2.3}$$

where $C_{p,s}$ is the heat capacity of the solid PCM, A_3 is the area defined by the integral in Equation 2.3, and T_r is the final temperature at the final time t_3. Note the arbitrary decision to use T_s as the temperature where solidification is complete as well as when it starts. This simplification is rectified in later implementations, as described below. Similar equations can be made for the standard (water):

$$(m_t C_{p,t} + m_w C_{p,w})(T_0 - T_s) = hA_c \int_{0}^{t_1'} (T - T_{\infty,a})\ dt = hA_c A_1' \tag{2.4}$$

$$(m_t C_{p,t} + m_p C_{p,w})(T_s - T_r) = hA_c \int_{t_1'}^{t_2'} (T - T_{\infty,a})\ dt = hA_c A_2' \tag{2.5}$$

where m_w is the mass of the water, $C_{p,w}$ is the heat capacity of the water, and t_1' and t_2' are the times the standard reaches T_s and T_r. Solving Equations 2.1–2.5 for $C_{p,s}$, $C_{p,l}$, and ΔH_m gives:

$$C_{p,s} = \frac{m_w C_{p,w} + m_t C_{p,t}}{m_p} \frac{A_3}{A_2'} - \frac{m_t}{m_p} C_{p,t} \tag{2.6}$$

$$C_{p,l} = \frac{m_w C_{p,w} + m_t C_{p,t}}{m_p} \frac{A_1}{A_1'} - \frac{m_t}{m_p} C_{p,t} \tag{2.7}$$

$$\Delta H_m = \frac{m_w C_{p,w} + m_t C_{p,t}}{m_p} \frac{A_2}{A_1'} (T_0 - T_s). \tag{2.8}$$

This analysis makes several assumptions which introduce error into the results that later studies have attempted to correct[30, 31, 32, 33, 34, 35, 36]. The first iteration of the T-history method assumes that the natural convective heat transfer coefficient is constant with changing temperature, but it actually is proportional to $T^{1/4}$ [33]. It also does not account for the temperature change of the liquid and solid phases during the solidification process. This would be fine if solidification actually was isothermal, but usually there is some amount of cooling during phase change. This problem is accounted for by adding a term for the heat capacities of the liquid and solid components to Equation 2.8 [32, 36].

Another problem arises because it is difficult to select the time when solidification is complete, particularly if the material being studied is impure. Hong *et al.* [32] proposed using the inflection point of the temperature versus time to find the point where solidification is complete as shown in Figure 2.3. Those authors justify this choice because during the phase transition there is a constant or slow decrease in temperature, but once the phase transition has stopped there is a rapid decrease in temperature. For all the samples studied in this thesis it was clear when solidification began because they all supercooled, and the temperature rose when the solidification had begun. In this thesis the time for total solidification, t_2, was found using the inflection point in the way Hong *et al.* proposed. In their work Marín *et al.* [33] noted that the original formulas could be reworked to use the concept of the variation of enthalpy with respect to temperature rather than the relationship of temperature and time. The variation of temperature over a small range, ΔT_i, corresponds to some time interval for the PCM, $\Delta t_i = t_{i+1} - t_i$, and for the standard, $\Delta t'_i = t'_{i+1} - t'_i$. Using this convention, Equations 2.1–2.5 can be simplified to

$$m_p \Delta h_p(T_i) + m_t c_{p,t}(T_i)(T_i - T_{i+1}) = hA_c \int_{t_i}^{t_i+\Delta t_i} (T - T_\infty)\, dt = hA_c A_i \tag{2.9}$$

$$(m_t C_{p,t}(T) + m_w C_{p,w}(T))(T_i - T_{i+1}) = hA_c \int_{t'_i}^{t'_i+\Delta t'_i} (T - T_\infty)\, dt = hA_c A'_i \tag{2.10}$$

where $\Delta h_p(T_i)$ and $C_p(T_i)$ are the temperature-dependent enthalpy change and heat capacity, respectively, in the range ΔT_i, and T_i is the average temperature in that range. Solving for $\Delta h_p(T_i)$ gives:

$$\Delta h_p(T_i) = \frac{m_w C_{p,w}(T_i) + m_t C_{p,t}(T_i)}{m_p} \frac{A_i}{A'_i} \Delta T_i - \frac{m_t}{m_p} C_{p,t}(T_i) \Delta T_i. \tag{2.11}$$

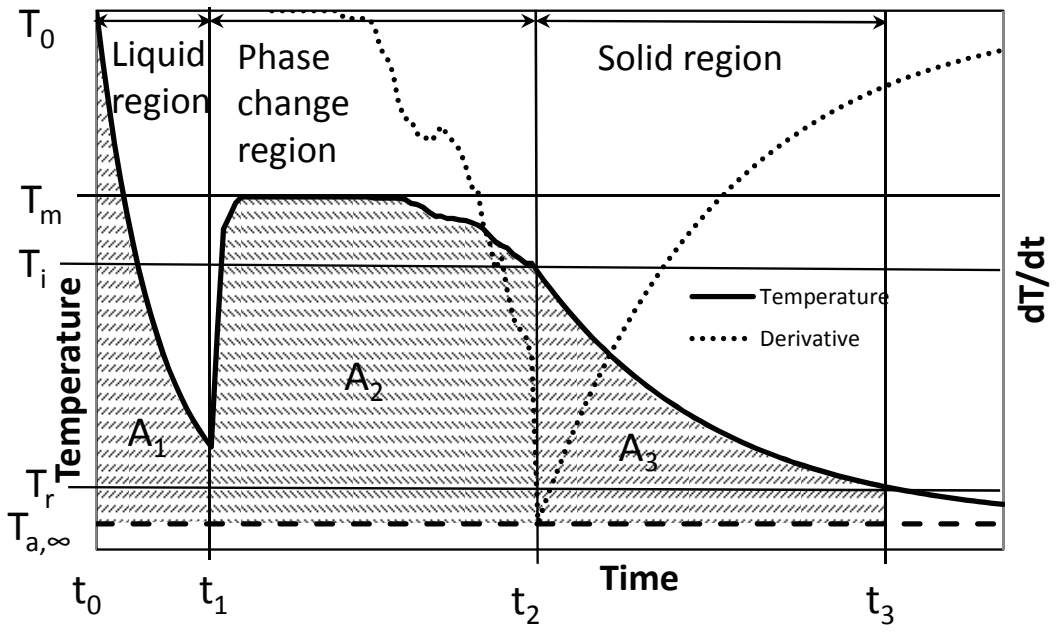

Figure 2.3: A modified version of Figure 2.1. As in that figure, in the A_1 area only liquid is present. After t_1, in A_2, solidification has started and liquid and solid are present together. Between t_2 and t_3, in A_3, only solid remains and the material rapidly cools toward ambient temperature. However, the inflection point of the temperature vs. time curve is used to determine solidification temperature, in this figure called inflection temperature, T_i. Accordingly, A_3 is proportionally larger, and there is a rational basis for establishing when solidification is complete.

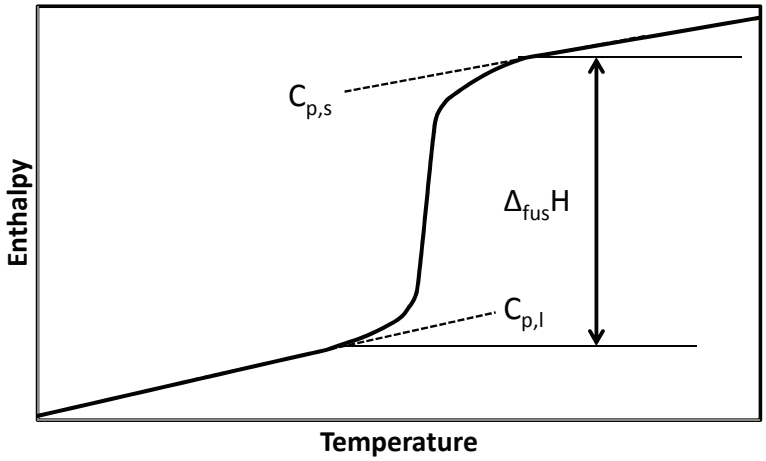

Figure 2.4: An example graph of enthalpy change versus temperature from T-history experiments for a phase change material. It is easy to see where the phase change occurs. The enthalpy of fusion can be measured by the jump in the graph as shown and the heat capacities of the solid and liquid correspond to the slopes before and after the phase change, respectively. This material exhibits no supercooling.

One of the most useful features of this improvement to the T-history method is the ability to use temperature dependent heat capacities and convective heat transfer coefficients.

The preferred way to represent T-history data is as enthalpy change versus temperature. This is done by picking an initial relative enthalpy for some T_i and then summing all previous enthalpies up to the current T_i. The graph that results from this process clearly and succinctly represents the important material characteristics. The phase transition enthalpy and phase change temperature range can be determined by the height and temperature interval of the steep part of the graph. The heat capacities of the liquid and solid are the slopes of the lines above and below the phase transition. The degree of the material's supercooling can also be determined with a quick assessment by observing the amount the temperature dips before the steep phase change region. An example is shown in Figure 2.4.

Out of the many improvements to the original T-history method that have been made, specifically the improvements made by Marín *et al.* [33] were chosen to best solve the particular difficulties found in the samples studied in this work. This method was selected because it integrates over each small data section and it is not necessary

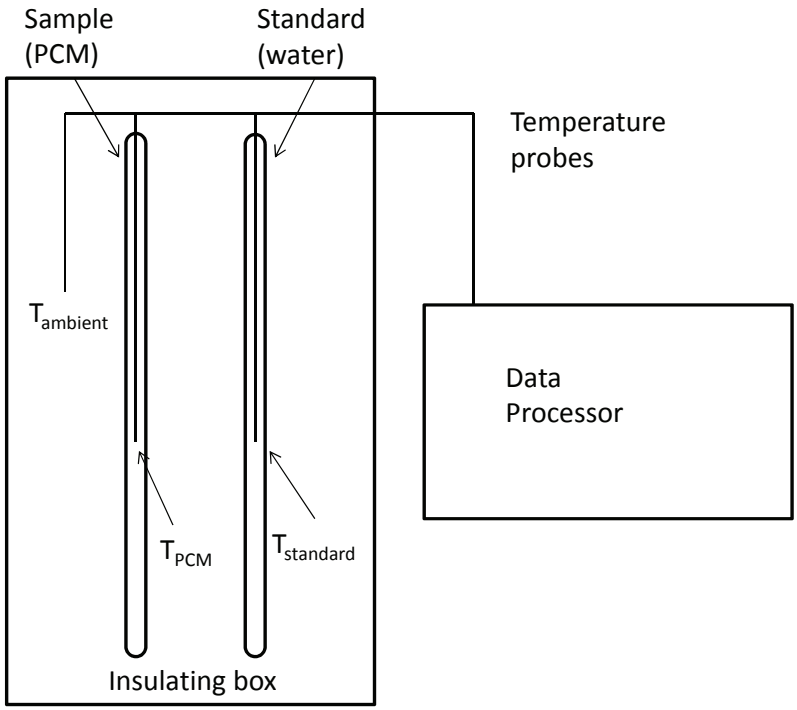

Figure 2.5: A schematic representation of the apparatus used to conduct T-history experiments.

to pick points along the cooling curve. This is helpful because those points may or may not accurately represent the start or end of each section. This is particularly true for materials that supercool or have large mushy regions during the phase change. This analysis also lends itself to easy presentation in the form of relative enthalpy versus temperature.

A box insulated with expanded polystyrene was used to house all samples. The measurement apparatus is shown schematically in Figure 2.5. Tubes were 30 cm long with inner diameter of 0.8 cm and outer diameter of 1 cm. This was narrow enough to satisfy the condition where the Biot number is less than 0.1, which allows the temperature distribution in the sample to be regarded as uniform. The Biot number is given by,

$$Bi = \frac{hR}{2\kappa} \tag{2.12}$$

where R is the radius of the tube, κ is the thermal conductivity, and h is the natural convective heat transfer coefficient of air outside the tube [29]. Although the values for h and κ were not known, the approximate range for the values was known. With

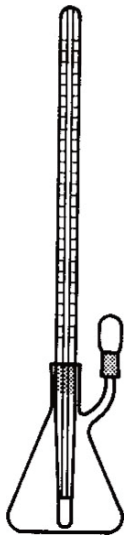

Figure 2.6: A schematic drawing of a pycnometer. By calibrating with a known standard the exact volume of the flask can be determined. Unknown liquid densities can then be determined by weighing the flask before and after adding a known volume of the material under investigation.

an h of between 5-10 W m^{-2} K^{-1}, and a radius of 0.008 m, the Bi is less than 0.1 when κ is greater than 0.2 to 0.4 W m^{-1} K^{-1}, which is a typical value for most salt hydrates [29]. Unshielded T-type thermocouples (uncertainty of $\pm$ 1 K) with diameter of 0.25 mm from OMEGA engineering were placed inside tubes so the tips were in the PCM and not contacting the walls of the tubes. An additional T-type therocouple was placed symmetrically between the tubes to measure the ambient temperature of the box. A National Instruments (NI) CompactDAQ, NI-cDAQ-9174, with 2 NI 9211 modules, was used to record the data. Parafilm was used to seal the top of the tube. The masses of the tubes were measured before and after adding the PCM. Tubes were oriented vertically and symmetrically so that radiation and convection between and around the tubes would be nearly equivalent.

2.5 Pycnometer

A glass pycnometer, nominally 25 mL, was used to measure the density of liquid $FeCl_3{\cdot}6H_2O$. A schematic drawing of the pycnometer is shown in Figure 2.6. The pycnometer was weighed empty, then filled at room temperature with supercooled liquid $FeCl_3{\cdot}6H_2O$, and then heated in a warm water (*ca.* 50 ℃) bath. At the

measurement temperature the pycnometer was removed from the bath. Since the liquid inside expands with increasing temperature a bead of liquid formed on the overfill spout of the pycnometer. The bead was carefully removed using an absorbent paper wipe and then the mass of the full pycnometer was taken again. By calibrating with a liquid of known density (water) it was possible to determine the volume of the pycnometer at various temperatures. Using the mass measured and the volume of the pycnometer it was then possible to measure the density of the unknown material. The density of the liquid was measured at 36.2 and 38 ℃. Although $FeCl_3 \cdot 6H_2O$ has a melting point of 37 ℃, because it supercools, it was possible to measure at temperatures lower than 37 ℃.

Chapter 3

Materials Characterization

3.1 Introduction

The materials presented here were not all characterized using the same methods. Depending on the literature information available and the unique character of each material several different experiments were performed. For $K_3PO_4 \cdot 7H_2O$, since very little is known about it, and since there are many related potassium/phosphate hydrates, a phase diagram was assembled. $FeCl_3 \cdot 6H_2O$ supercooled and had slow crystal growth, so a search for suitable nucleating agents was performed. Also the liquid density was measured since no value was available in the literature. In the case of $Mn(NO_3)_2 \cdot 4H_2O$, since it is relatively well behaved only DSC, TGA, and T-history measurements were performed.

3.2 $K_3PO_4 \cdot 7H_2O$

3.2.1 Phase Diagram

When dealing with phase transitions in hydrates, a salt/H_2O phase equilibrium diagram is an extremely useful tool as it shows the relationships between the phases at different mass percentages and temperatures. In the case of salt hydrates, solubility information can be used to create a phase diagram. New solubility measurements were not required because considerable information about K_3PO_4 and its solubility in water was available in the literature [37]. Using the data and knowing the phase rule made it possible to construct a phase equilibrium diagram. Figure 3.1 shows the phase diagram with reasonable estimates included. Estimates were needed because the solubility data lack information about the solubility curves between the trihydrate and the heptahydrate. This represented a very small section of the phase diagram, and although more measurements would be useful, since high precision and accuracy would be needed, no solubility measurements were performed. However,

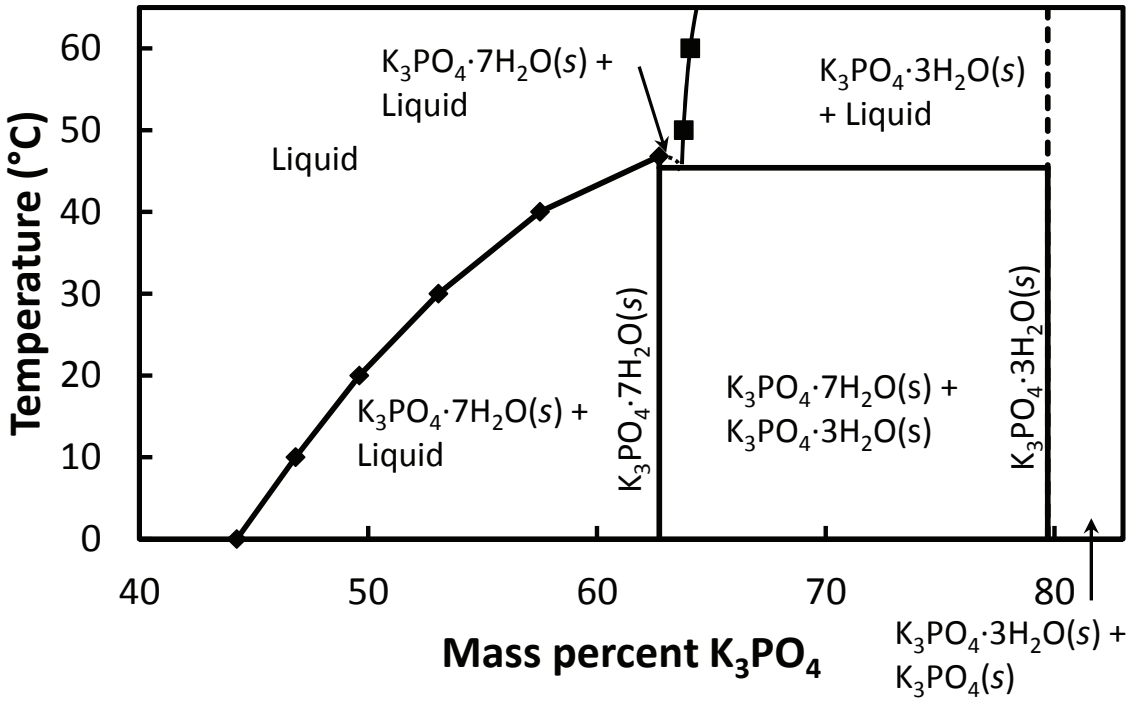

Figure 3.1: Partial phase equilibrium diagram of K_3PO_4 and H_2O. The eutectic is known to be at 45.5 ℃ [38], but no data are available for solubility curves between $K_3PO_4 \cdot 3H_2O$ and $K_3PO_4 \cdot 7H_2O$. Dashed lines do not represent data, but are guides for the eyes and reasonable estimates.

this section of the phase diagram is important and future work should address it. Additionally, the decomposition/melting point of the trihydrate is not known. The eutectic temperature for $K_3PO_4{\cdot}3H_2O$ and $K_3PO_4{\cdot}\ 7H_2O$ is 45.5℃ [38].

The diagram shows the importance of keeping the amount of water stable in a PCM system, because even small losses, specifically about 0.3 H_2O per mole of K_3PO_4 or about 2% by mass, can lead to trihydrate formation. The formation of $K_3PO_4{\cdot}3H_2O$ is undesirable because the trihydrate has a much higher melting temperature and its presence would therefore decrease the performance of the PCM. As mentioned before, it is not known how much higher the melting point for $K_3PO_4{\cdot}3H_2O$ is, but the slope of the points in Figure 3.1 indicates a relatively high melting temperature, certainly outside the range of most solar thermal PCM systems.

To further understand the system it can be advantageous to add a third dimension to the phase diagram. Potassium oxide (K_2O), phosphorus pentaoxide (P_2O_5), and water (H_2O) together form a pseudoternary phase equilibrium diagram that can be informative when studying $K_3PO_4{\cdot}7H_2O$ and related compounds. Wendrow and Kobe [38] collected data on this system and from their data a ternary diagram was constructed here; it is shown in Figure 3.2. Each point on the diagram corresponds to a specific compound such as $K_3PO_4{\cdot}7H_2O$. A line from that point to the H_2O vertex represents changing the amount of water while keeping the ratio of K_2O to P_2O_5 fixed. This line represents what happens if water evaporates from the system and passes through any other hydrates of the same K_2O/P_2O_5 ratio. Contour lines at various temperatures complete the picture, providing understanding of what happens at specific temperatures. Although the data available in the literature are limited [38], they still provide valuable information; for instance, the melting point and melting behavior of a compound can be determined. This phase diagram shows that $K_3PO_4{\cdot}7H_2O$ does indeed melt congruently, and it also shows a few other potassium-phosphate hydrates that could be of interest for use as PCMs. For example, $K_2HPO_4{\cdot}6H_2O$ also melts congruently below 25 ℃, which could be of interest for thermal regulation in living environments.

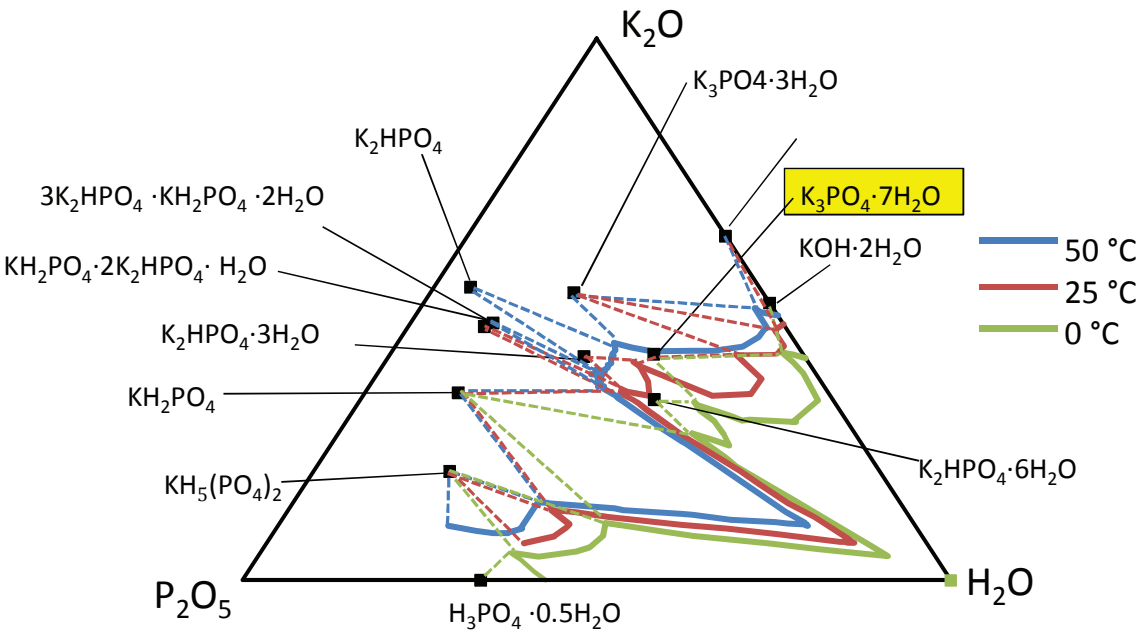

Figure 3.2: A mass percent ternary diagram for K_2O, P_2O_5, and H_2O at 0 ℃, 25 ℃, and 50 ℃. Dashed lines indicate approximate areas where a specific solid would be present and which sections of the solubility curve corresponds to which material. Black symbols (■) are exact compositions of the indicated materials.

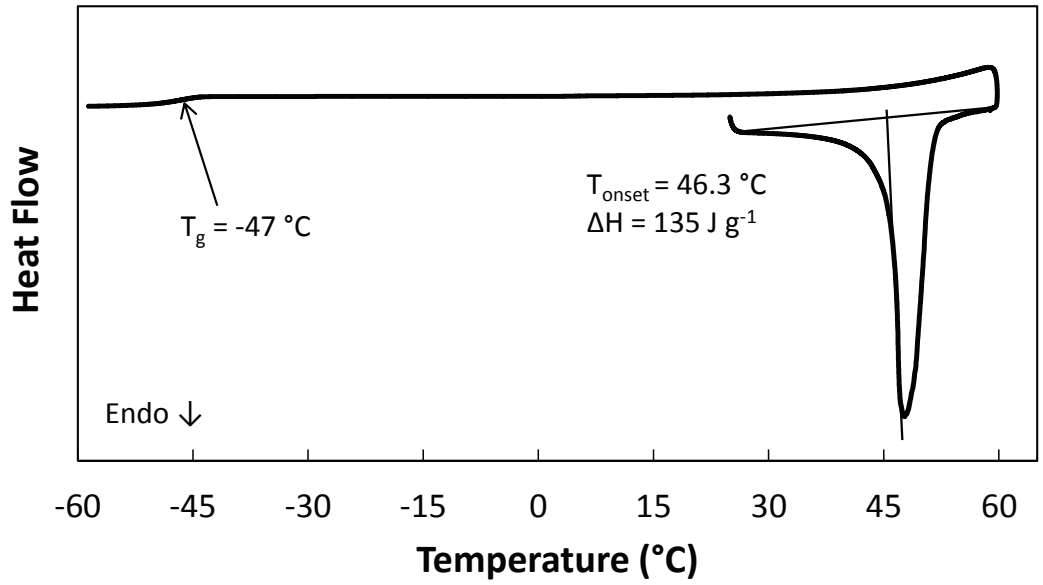

Figure 3.3: An example of a typical DSC curve for $K_3PO_4{\cdot}7H_2O$ performed at 5 K min^{-1}. A melting peak is present at 46.3 ℃, but no freezing occurs. A glass transition can be seen at -47 ℃.

3.2.2 TGA Results

The hydration number of $K_3PO_4{\cdot}7H_2O$ was determined to be 7.02 ± 0.04 by thermogravimetric analysis. Three replicates were measured all having similar mass of approximately 45 mg. The value is close enough to 7 that the melting point should not be affected significantly. This amount of water comes to a difference of 0.07 mass percent, which it is too small a difference to be discerned on the diagram of Figure 3.1.

3.2.3 DSC Enthalpy Change

Using DSC at a heating rate of 10 K min^{-1} the enthalpy of fusion for $K_3PO_4{\cdot}7H_2O$ was determined to be 132 ± 4 kJ kg^{-1} (288 ± 9 kJ L^{-1})* with four replicates with an average mass of 9.8 mg. The melting temperature was determined to be 46.81 ± 0.05 ℃ based on two replicates, from the onset temperature using a heating rate of 1 K min^{-1}. An example curve is shown in Figure 3.3. Supercooling was severe enough that no freezing was seen in the present study. In fact, it was possible to supercool

*Based on solid density of 2.18 kg L^{-1}.

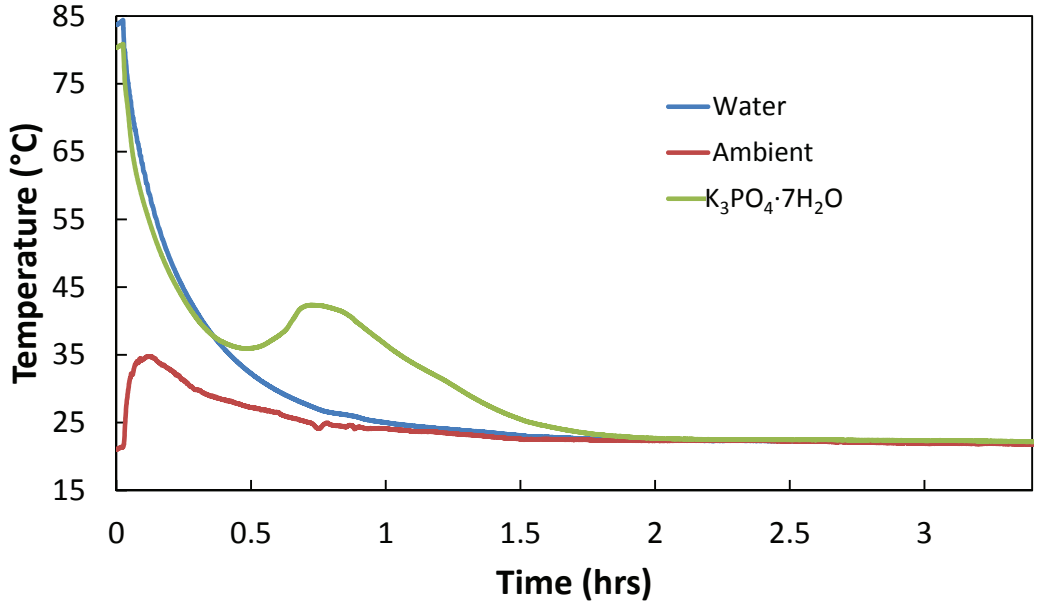

Figure 3.4: This graph shows a typical cooling curve for T-history measurements for a 35 g sample of $K_3PO_4{\cdot}7H_2O$. While the standard, water, cools asymptotically towards the ambient temperature, the phase change material stays at a higher temperature much longer. Note the supercooling that occurs around the 0.5 hour mark.

even at moderate cooling rates (5 K min^{-1} cooling gave a glass transition point at about -47 ℃).

3.2.4 T-history Enthalpy Change

A typical T-history cooling curve for $K_3PO_4{\cdot}7H_2O$ is shown in Figure 3.4. Enthalpy of fusion was measured with three replicates, of mass of about 40 grams, and determined to be 125 ± 4 kJ kg^{-1} (273 ± 9 kJ L^{-1}).* This value is very close to the measured value from the DSC, which is somewhat surprising given that the systematic error of the T-history method is anticipated to be fairly high. Zhang *et al.* showed that error was given by

$$\frac{\Delta H_m}{H_m} \approx \frac{4\Delta T}{T_m - T_{\infty,a}} + \frac{2\Delta T}{T_0 - T_m}, \tag{3.1}$$

where ΔT is the uncertainty of the temperature measurement. With ΔT being 1 K, the average value for the error was 22% which as stated before is much higher than

*Based on a solid density of 2.18 kg L^{-1}.

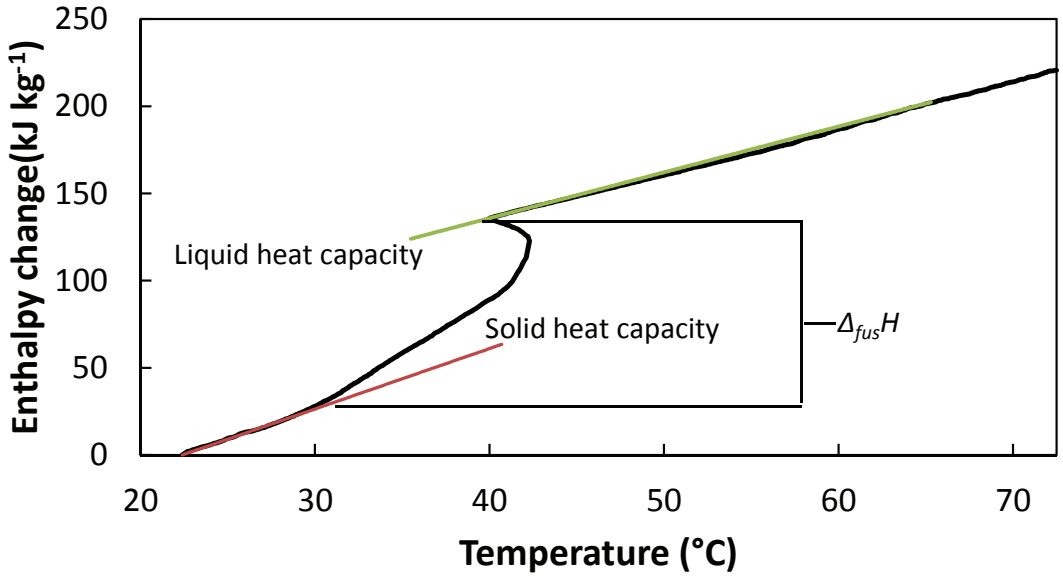

Figure 3.5: An enthalpy change versus temperature T-history result for $K_3PO_4{\cdot}7H_2O$. The heat capacities of the liquid and solid states were determined by fitting linear trendlines to the liquid and solid regions. Although C_p will change as a function of temperature it remains roughly constant over a limited temperature range. Enthalpy change of the transition was directly determined by the region between completely liquid and completely solid.

the statistical error ($\pm$ 4 kJ kg^{-1}) given above. Average heat capacities of liquid and solid were found to be 2.7 $\pm$ 0.2 kJ kg^{-1} K^{-1} and 3.1 $\pm$ 0.5 kJ kg^{-1} K^{-1} respectively. The high error for the solid can be accounted for by the fact that it becomes difficult to assess differences in area accurately when the standard, ambient, and sample are all very close in temperature. Since the uncertainty of the measurement is comparable to the difference in the temperature, it means that the uncertainty in the determination becomes greater.

An example of the enthalpy change versus temperature graph that was used to determine the parameters is shown in Figure 3.5. During some measurements the temperature probe corroded slightly and the measured temperatures were inaccurate. Because the tests were run for a time before and after all the samples had reached thermal equilibrium it was possible to do a correction. A linear correction factor was applied to the whole temperature range using the equilibrium temperatures as a baseline.

Table 3.1: A list of materials that match the lattice parameters of $FeCl_3 \cdot 6H_2O$ within 15% and share the monoclinic crystal structure. These materials were considered as potential nucleators for $FeCl_3 \cdot 6H_2O$.

Material	Chemical Formula	a (Å)	b (Å)	c (Å)	β	Reason for ruling out
$FeCl_3 \cdot 6H_2O$	$FeCl_3 \cdot 6H_2O$	11.834	7.029	5.9524	100.47°	N/A
Koktaite	$(NH_4)_2Ca(SO_4)_2 \cdot H_2O$	10.17	7.15	6.34	102.75°	Soluble
Omongwaite	$Na_2Ca_5(SO_4)_6 \cdot 3H_2O$	12.08	6.96	6.39	90.2°	Soluble
Bassanite	$CaSO_4 \cdot .5H_2O$	12.03	6.92	12.67	90.27°	Soluble
Syngenite	$K_2Ca(SO_4)_2 \cdot H_2O$	9.77	7.14	6.25	104.01°	Soluble
Edgarbaileyite	$Hg_6Si_2O_7$	11.72	7.69	5.96	112.07°	Contains Hg

3.2.5 Discussion

$K_3PO_4 \cdot 7H_2O$ looks to be a promising phase change material. Although it exhibits supercooling, once nucleated, crystal growth is rapid, as can be seen by the cooling curve in Figure 3.4. The relatively low energy density (130 kJ kg^{-1}) is offset by the high solid density of the material (2.18 kg L^{-1}), at least compared to organic PCMs (typically around 1 kg L^{-1}). As a result, the volumetric energy density (283 kJ L^{-1}) is high enough to warrant further research. Also note that the anhydrous form is already a mass-produced product for the food industry [39]. This means that a market is already established and the cost is relatively low at around $1000–2000 per tonne for the bulk commodity [40].

3.3 $FeCl_3 \cdot 6H_2O$

3.3.1 Nucleation Agent Search

Preliminary tests and observations of $FeCl_3 \cdot 6H_2O$ indicated that it supercooled easily and crystallized slowly. In an attempt to look for solutions to these issues, the computer software Match! [41] was used to find materials that were of the same crystal structure as $FeCl_3 \cdot 6H_2O$ and with lattice parameters within 15% of it [42] to act as potential nucleation agents for it. Several materials were found that fit the parameters, but many of them were not suitable for various reasons, such as containing toxic elements, being volatile, or decomposing at elevated temperatures or in the presence of water. See Table 3.1 for the list considered. The best candidates found were a class of similar minerals related to gypsum ($CaSO_4$).

A small quantity of a mixed ammonium calcium sulfate salt was synthesized using ammonium sulfate and calcium nitrate. A solution of calcium nitrate was added to saturated solution of ammonium sulfate. Because gypsum, koktaite, and other $CaSO_4$ relatives are considerably less soluble in water than ammonium sulfate and calcium nitrate, they precipitate out of solution. When added to molten supercooled $FeCl_3{\cdot}6H_2O$ at room temperature, the synthesized salt quickly dissolved and no nucleation was observed. Being so readily soluble in $FeCl_3{\cdot}6H_2O$, the related family of $CaSO_4$ salts were discarded as candidate nucleating agents. Ultimately, no suitable nucleation agents were identified.

3.3.2 Density Measurement

The density of $FeCl_3{\cdot}6H_2O$ at 38 ℃, just above the melting point ($T_m = 37$ ℃), was measured with seven replicates and found to be 1.6455 ± 0.0002 kg L^{-1}. With two replicates at 36.2 ℃, below the melting point, the liquid density was found to be 1.65 ± 0.03 kg L^{-1}.

3.3.3 DSC Enthalpy Change

Enthalpy measurements were difficult because $FeCl_3{\cdot}6H_2O$ reacted with the Al pans used in the DSC at temperatures slightly above the melting point. With two replicates the enthalpy of fusion measured was 168 ± 11 kJ kg^{-1}(276 ± 18 kg L^{-1}).* Onset temperature was 40.9 ± 0.6 ℃. The results available show a smaller $\Delta_{fus}H$ and higher melting temperature than values (223 kJ kg^{-1}, 37 ℃) reported by Sharma *et al.* [9].

3.3.4 T-history Enthalpy Change

The cooling curve for $FeCl_3{\cdot}6H_2O$ was quite atypical. Usually, for materials that supercool, the curve looks similar to the one shown in Figure 3.4 where the liquid cools below the melting temperature and then spontaneously nucleates or is otherwise seeded. Most often, once the crystallization begins, the temperature immediately climbs to nearly the melting point of the solid, holds roughly at the melting temperature until most of the liquid has crystallized, and then begins to cool to ambient temperature. However, $FeCl_3{\cdot}6H_2O$ does not follow this trend and the curve appears

*Calculated from liquid density measured in this thesis.

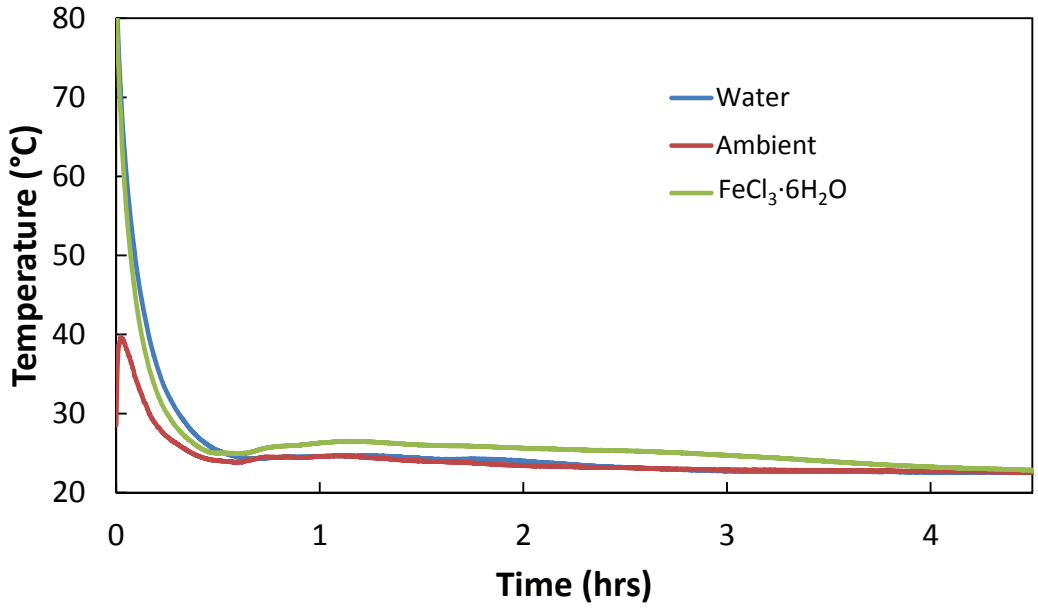

Figure 3.6: A T-history cooling curve for $FeCl_3 \cdot 6H_2O$. The temperature barely rose above ambient and did not even approach the melting temperature at 37 ℃.

as shown in Figure 3.6. Even when the sample was seeded, the temperature did not jump up to just below the melting point. Instead the crystals slowly formed and released heat over a long period of time, causing the temperature to hover slightly above ambient. This is rather unusual as typically if a solid is in equilibrium with its liquid form it must be at the melting temperature. This anomaly arises because of the slow crystal growth rate and the way the thermocouple measures the temperature. Although in the immediate vicinity of the crystallization front the temperature must be at the melting point, the area of crystallization is so small compared to the bulk, that the temperature farther away quickly approaches ambient.

The anomalous temperature curve posed some problems for measurement, but, given sufficient time, the T-history method was still able to get an estimate of the $\Delta_{fus}H$ and heat capacity of the liquid. As can be seen from Figure 3.6, the $FeCl_3 \cdot 6H_2O$ temperature was consistently higher than the water and ambient and therefore a difference in area could be compared. The enthalpy of fusion and the liquid heat capacity were found to be 231 kJ kg^{-1} (380 kg L^{-1})* and 2.1 kJ kg^{-1} K^{-1},

*Calculated from liquid density measured in this thesis.

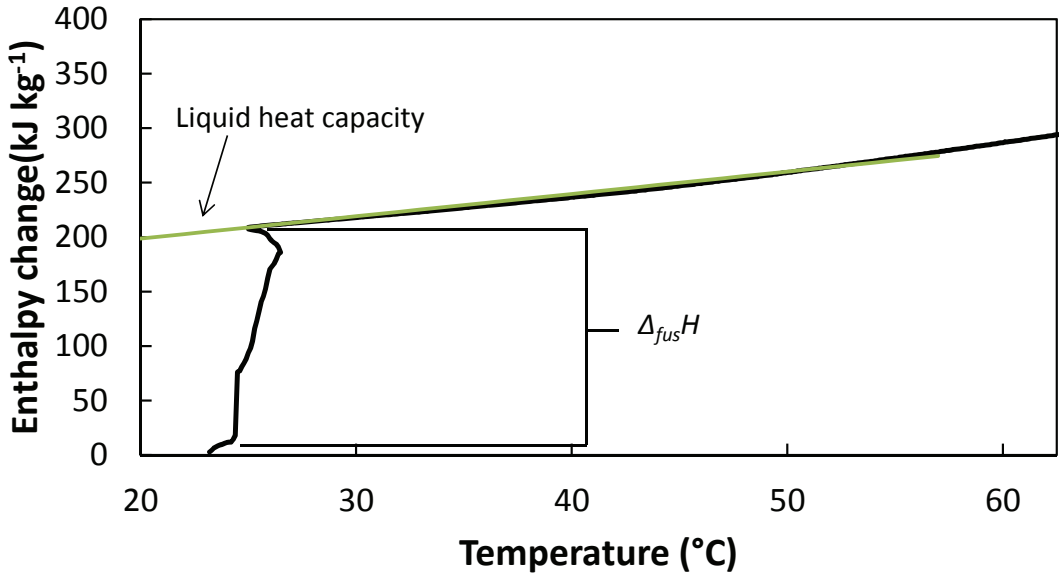

Figure 3.7: An enthalpy change versus temperature T-history result for $FeCl_3{\cdot}6H_2O$. The heat capacities of the liquid state was determined by fitting a linear trendline to the liquid region. Although C_p will change as a function of temperature it remains roughly constant over a limited temperature range. Enthalpy change of the transition was directly determined by the region between completely liquid and completely solid.

respectively, with one measurement. The ΔH vs. T graph is shown in 3.7.

3.3.5 Discussion

Despite its high $\Delta_{fus}H$ (223 kJ kg^{-1} [9], 368 kJ L^{-1})* $FeCl_3{\cdot}6H_2O$ is not a promising candidate material for thermal energy storage. The liquid phase was observed to be viscous, estimated to be similar to mineral oil. This feature of the liquid phase combined with the high $\Delta_{fus}H$ make for very unfavorable crystal growth. The problem of supercooling means that when $FeCl_3{\cdot}6H_2O$ has melted, the thermal energy is virtually impossible to extract without a nucleation aid. And then even when a seed crystal is introduced the crystal growth rate is extremely slow, taking about 4 to 6 hours to fully crystallize for a mass of around 50 g. Therefore, if a suitable nucleating agent were found it would need to be very well dispersed so that nucleation would happen in a reasonable amount of time. $FeCl_3{\cdot}6H_2O$ is also more corrosive than many other

*The volumetric energy given here was calculated using the liquid density measured in this thesis. Since in this thesis an accurate assessment of the $\Delta_{fus}H$ of $FeCl_3{\cdot}6H_2O$ was not able to be measured, the literature value was used [9].

salt hydrates as can be seen from the fact that it reacted with the aluminum pan and the copper and constantan thermocouple.

3.4 $Mn(NO_3)_2{\cdot}4H_2O$

3.4.1 DSC Enthalpy change

When the $\Delta_{fus}H$ of $Mn(NO_3)_2{\cdot}4H_2O$ was measured a few interesting effects were observed. On the first cycle $Mn(NO_3)_2{\cdot}4H_2O$ was found to have a $\Delta_{fus}H$ of 125 ± 2 kJ kg^{-1} (266 ± 4 kJ L^{-1})* and an onset temperature of 36.0 ± 0.6 ℃. Three replicates were performed each with a mass of about 9 mg. Further cycling gave an $\Delta_{fus}H$ of 94 ± 1 kJ kg^{-1} and an onset temperature of 37.0 ± 0.3 ℃. Thirteen replicates of the repeated cycling were performed. This decrease is probably the result of the formation of a different compound than the tetrahydrate after the first melting. It is also possible that the manganese ions reacted with the aluminum pan by the reaction $3Mn^{2+}(aq) + 2Al(s) \rightarrow 3Mn(s) + 2Al^{3+}(aq)$. But because the standard electrode potential for this reaction is negative (3(-1.185 V)+ 2(1.662 V) = -.231 V) [6], that means this reaction is not spontaneous and this reaction probably did not occur. Maximum temperature of the experiments was typically around 50 ℃ and never went higher than 100 ℃.

During T-history measurements and other experiments with larger samples, on the order of 60 g, it was observed that occasionally instead of crystallizing in light pink crystals as they initially appeared, yellow crystals would form. Hexa- and monohydrates are known to form with manganese nitrates. But according to literature the hexahydrate and mixed hydrates of manganese nitrate are also pink [43], and since the onset temperature did not change greatly from the initial melting, hexa- and monohydrate are unlikely. More likely some amount of the sample precipitated out as anhydrous manganese nitrate and did not participate in the melting/freezing cycles in subsequent cycles. It was observed that onset temperature for freezing decreased every subsequent cycle, as can be seen in Figure 3.8. However, the enthalpy change on freezing did not follow a similar trend. In some cycles the enthalpy change on freezing decreased; in others it increased, as can be seen in Figure 3.9. The reason for the

*Calculated using solid density [25].

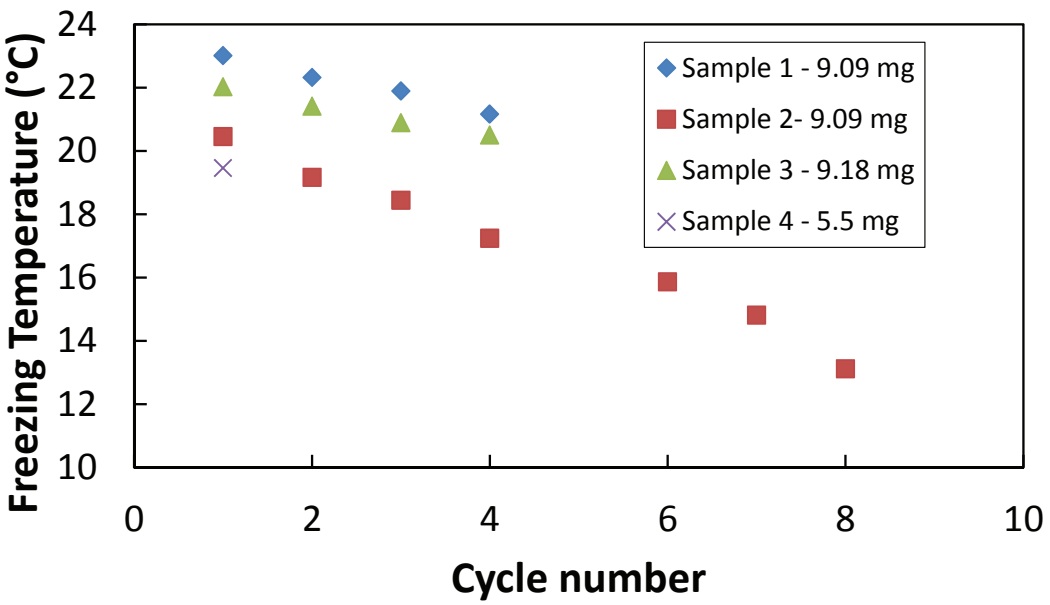

Figure 3.8: The freezing point of $Mn(NO_3)_2{\cdot}4H_2O$ tended to decrease with increasing cycles. Gaps in cycles are present because for some cycles freezing was not well enough behaved to measure the onset temperature accurately. Results for different samples are shown with different symbols.

trend of decreasing onset temperature of freezing is not readily apparent, although it may have something to do with the first measured $\Delta_{fus}H$ being consistently higher that the subsequent measurements.

3.4.2 T-history Enthalpy Change

A typical T-history cooling curve for $Mn(NO_3)_2{\cdot}4H_2O$ is shown in Figure 3.10. Using the T-history method the enthalpy of fusion was measured to be 170 ± 30 kJ kg^{-1} (380 ± 64 kJ L^{-1})* from three replicates. Average heat capacities of the liquid and solid were measured to be 2.6 ± 0.4 kJ kg^{-1} K^{-1} and 3.9 ± 0.9 kJ kg^{-1} K^{-1} respectively. The error is higher than for $K_3PO_4{\cdot}7H_2O$, although it is still in the region that would be expected for T-history measurements. The hexahydrate may have formed initially because the material dwelt at about 28 ℃ which is closest to the melting point of $Mn(NO_3)_2{\cdot}6H_2O$ (26.8 ℃) before increasing in temperature to the melting point of $Mn(NO_3)_2{\cdot}4H_2O$ at 37 ℃. A ΔH vs. T graph for one sample is shown in Figure 3.11.

*Calculated using solid density [25].

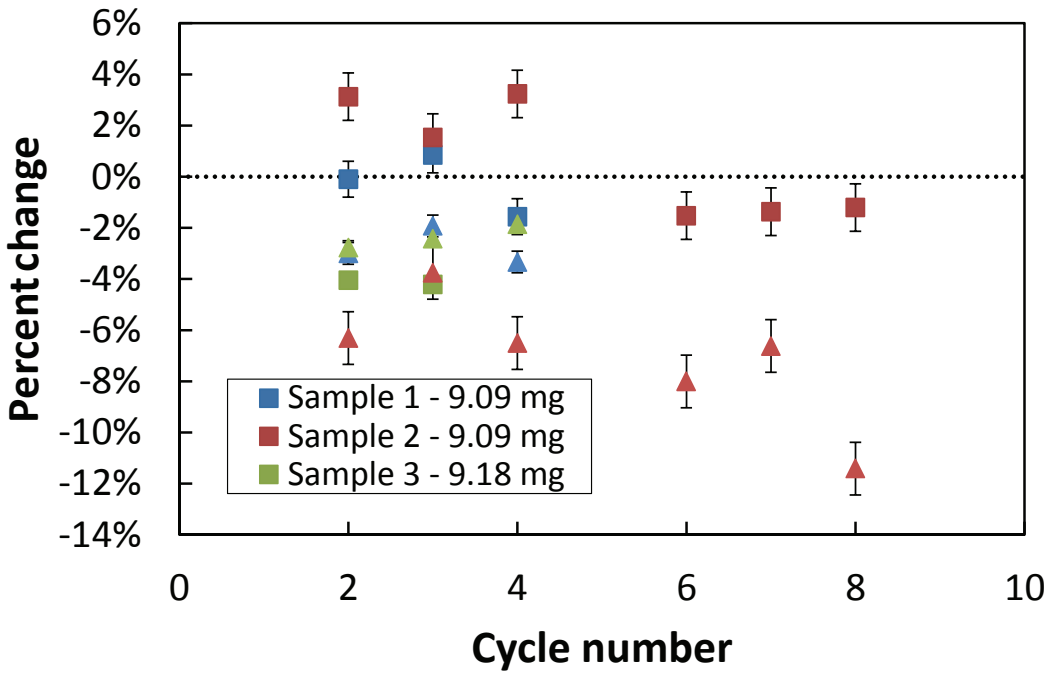

Figure 3.9: The percent sequential change of ΔH of freezing (■, ■, ■) and onset temperature of freezing (▲, ▲, ▲) from one cycle to the next. For onset temperature the percentage is always below zero. For ΔH the distribution is more random, falling above and below zero. Different colored points are separate samples.

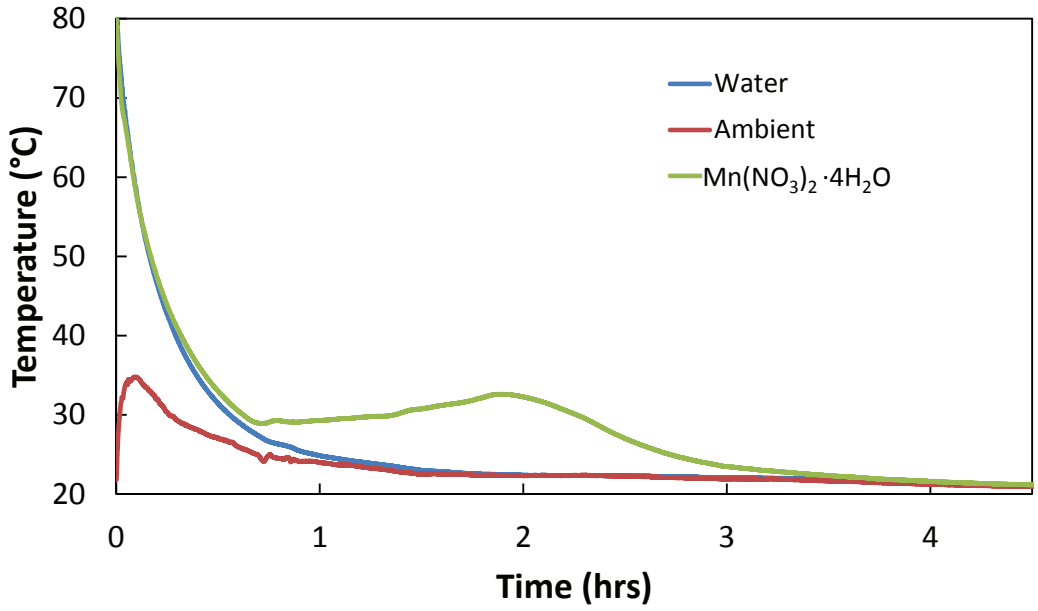

Figure 3.10: A typical cooling curve for T-history measurements for $Mn(NO_3)_2{\cdot}4H_2O$. While the standard, water, cools asymptotically towards the ambient temperature the phase change material stays at a higher temperature much longer, although some supercooling does occur.

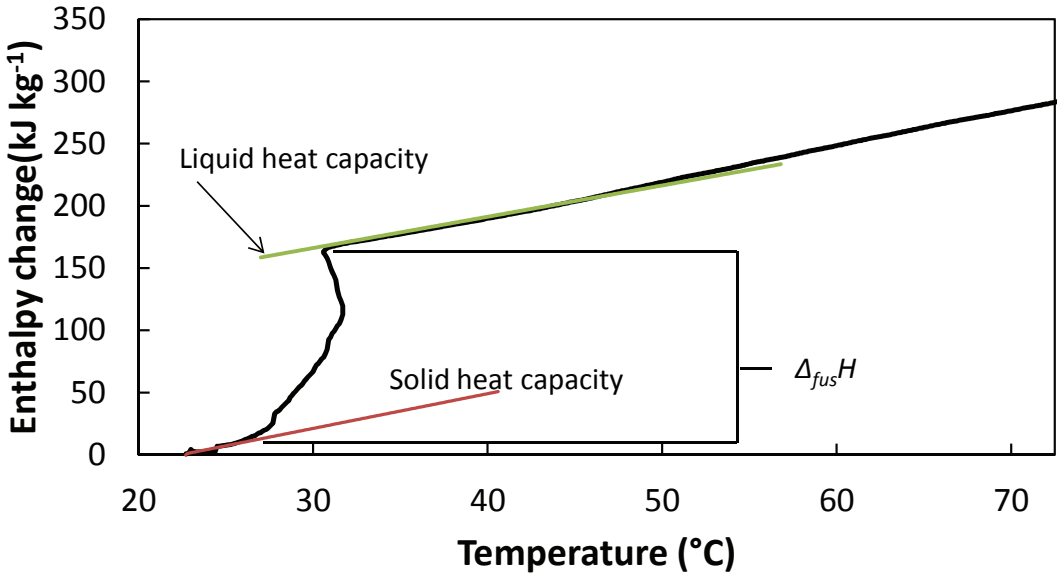

Figure 3.11: An enthalpy change versus temperature T-history result for $Mn(NO_3)_2{\cdot}4H_2O$. The heat capacities of the liquid and solid states were determined by fitting linear trendlines to the liquid and solid regions. Although C_p will change as a function of temperature it remains roughly constant over a limited temperature range. Enthalpy change of the transition was directly determined by the region between completely liquid and completely solid.

3.4.3 TGA

It was not possible to determine the exact hydration of $Mn(NO_3)_2{\cdot}4H_2O$ using TGA because it chemically decomposed before losing all its water of hydration. The samples decomposed above 100 ℃, which is well above the range of the DSC, so it is unlikely that DSC samples were decomposing in the same manner as in the TGA experiments.

3.4.4 Discussion

$Mn(NO_3)_2{\cdot}4H_2O$ is of uncertain potential as a PCM. Although on first appearance it seems to be a congruent melter in bulk, when measured in the DSC it seems to exhibit characteristics of an incongruent melting compound. It also has a relatively low $\Delta_{fus}H$. However, the low degree of supercooling is good for a salt hydrate and the material could warrant further research.

Table 3.2: A summary of the results in this chapter with literature values for comparison.

PCM	$\Delta_{fus}H$ (kJ kg^{-1}) DSC	$\Delta_{fus}H$ (kJ kg^{-1}) T-history	$\Delta_{fus}H$ (kJ kg^{-1}) Lit.	T_m (℃)	T_m (℃) Lit.
$K_3PO_4{\cdot}7H_2O$	132±4	125±4	N/A	46.81±0.05	45 [5]
$FeCl_3{\cdot}6H_2O$	168±11	231	223 [9]	40.9±0.6	37 [9]
$Mn(NO_3)_2{\cdot}4H_2O$	125±2	170±30	115 [9]	36.0±0.6	37.1 [9]

Table 3.3: A summary of the results in this chapter, presented volumetrically. Literature values are calculated from specific heats of fusion from literature using the density value in this table.

PCM	$\Delta_{fus}H$ (kJ L^{-1}) DSC	$\Delta_{fus}H$ (kJ L^{-1}) T-history	$\Delta_{fus}H$ (kJ L^{-1}) Lit.	Density (kg L^{-1})
$K_3PO_4{\cdot}7H_2O$	288±9	273±9	N/A	2.18 (solid)
$FeCl_3{\cdot}6H_2O$	276±18	380	368 [9]	1.6455 ±0.0002 (liquid)
$Mn(NO_3)_2{\cdot}4H_2O$	266±4	362±64	245 [9]	2.13 (solid) [25]

3.5 Summary of Results

Now that each material has been treated individually, it is useful to compare the results. The results are summarized in Tables 3.2 to 3.4 with literature values for comparison. Where literature values are available for heats of fusion they generally agree fairly well. The exception is the DSC value for $FeCl_3{\cdot}6H_2O$, which is low, most likely because of the exothermic reaction with the aluminum pan canceling out part of the endothermic phase change. The T-history method generally measured a greater specific heat capacity of the materials compared to literature values. As can be seen in Table 3.3 all three materials have a high volumetric heat of fusion.

Table 3.4: A summary of the heat capacity results in this chapter with literature values for comparison.

PCM	$C_{p,l}$ (kJ kg^{-1} K^{-1}) Lit.	$C_{p,s}$ (kJ kg^{-1} K^{-1}) Lit.	$C_{p,l}$ (kJ kg^{-1} K^{-1})	$C_{p,s}$ (kJ kg^{-1} K^{-1})
$K_3PO_4{\cdot}7H_2O$	N/A	N/A	2.7±.2	3.1±.5
$FeCl_3{\cdot}6H_2O$	N/A	1.02 [25]	2.1	Not measured
$Mn(NO_3)_2{\cdot}4H_2O$	N/A	1.04 [25]	2.6±.4	3.9±.9

Chapter 4

Life Cycle Assessment of Dodecanoic Acid in a Solar Thermal Energy Storage System

4.1 Introduction

Because a major goal of the development of PCMs is to provide an energy storage medium for environmentally friendly energy technologies, it is important to assess each material's environmental impact. It would be fruitless to develop a material which causes more problems in its manufacture than it solves in its use. For example, it is useless to develop a material to store thermal energy if it takes more energy to produce that material than it can store or if its manufacture emits excessive CO_2. In light of this, a life cycle assessment (LCA) of a promising phase change material, dodecanoic acid, as applied in a solar hot water system, was carried out.

A life cycle analysis endeavors to take all aspects of a product's manufacture, processing, use, and disposal into account and thereby assesses the environmental impact of the product. The environmental impact of a product is difficult to absolutely quantify, so an LCA usually quantifies key inputs and outputs, most often energy, water, and CO_2. A number of other pollutants such as SO_2 and NO_x also may be taken into account. Additionally, other environmental effects such as eutrophication can be included in an LCA.

To begin the LCA of a product, first an accurate life cycle inventory has to be established. For many materials literature is already available that gives the environmental impact, but such is not the case for dodecanoic acid. Therefore, a life cycle inventory of dodecanoic acid was established.

4.2 Dodecanoic Acid

Dodecanoic acid, commonly known as lauric acid, is a natural product that can be derived from three principal sources: the kernel of the oil palm, *Elaeis guineensis*;

the kernel, which is called the meat, of the coconut palm, *Cocos nucifera*; and from various animal fats known as tallow [20]. The present study focused on dodecanoic acid coming from the kernel of the oil palm. This source was chosen because palm kernel oil makes up the majority of the feedstock for dodecanoic acid production and also because oil palm has the lowest land use of any oil producing plant [44, 45].

This analysis draws from several life cycle analyses and industrial documents in its attempt to quantify the environmental impact of dodecanoic acid. A number of analyses and assessments have been carried out for palm oil and its potential as a biodiesel fuel source [46, 45, 44, 47, 48]. Although these analyses pertain to palm oil, because a fixed amount of palm kernel oil is produced at the same time as palm oil, it is possible to relate the energy use and CO_2 emission during production of dodecanoic acid to these studies.

4.2.1 Background

Oil palm is a valuable food plant originating in Africa. Both the kernel and the fruit of the tree are extremely rich in fats and oils [49]. The uses for the oils are wide, ranging from food, to detergent, to soap [20, 50]. Despite the oil palm's African origin, today most oil palm plantations are in Indonesia and Malaysia [50]. The high saturated fat content of the oils is useful because usually plant sources of oil are high in unsaturated fat. While unsaturated fat may be healthier as a food, as a chemical feedstock saturated fats have more uses. Additionally, with the phasing out of trans fats from many food markets, there has been an increase in demand for fats and oils that are solid at room temperature, and palm kernel oil is solid [51].

There are three main stages associated with the production of dodecanoic acid: the agricultural stage, encompassing the land use and cultivation of oil palms; the milling stage, where the crude oil is formed; and the fatty acid splitting and distillation stage. Figure 4.1 shows a schematic diagram of the system boundaries.

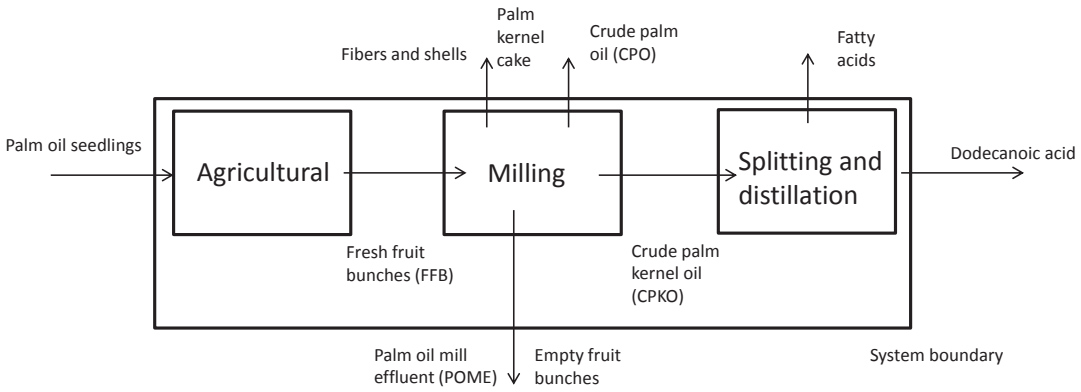

Figure 4.1: System boundaries for the dodecanoic acid LCA.

4.2.2 Palm Oil Production

Land Use and Agricultural Phase

Before oil palm plantations can produce fruit, the land has to be cleared. In Malaysia and Indonesia, land is usually cleared through slash and burn methods. Clearly these methods have a high environmental cost, both in terms of the CO_2 released and the ecosystem degradation.

Once the land is clear, various leguminous cover plants are planted to help nitrogenate the soil [45, 52]. Oil palm seedlings grown elsewhere in greenhouses are transplanted into the soil [53]. The seedlings are then cultivated and fertilized until, after a number of years, the plants reach maturity and start producing fruit. The seedlings were excluded from this study because their contribution to the total embodied energy and CO_2 emissions were negligible [53]. The fruit forms in bunches, called fresh fruit bunches (FFB) in the industry, which after harvesting are taken immediately to the palm oil mill to prevent deterioration of the oil [45].

Milling

At the oil mill a number of processes are undertaken to extract oil from the fruit and remove the kernel. The process starts with sterilization, where the FFBs are treated with steam to loosen the fruitlets from the bunch and deactivate enzymes that change the oil to free fatty acids [54]. (Although in the case of this study a free fatty acid is a

desirable end product, for most purposes the crude oil is the most valuable product.) The FFBs are fed into a rotary drum which strips the fruits from the bunches. The empty bunches are either composted or burned in the mill to produce the steam needed for sterilization [54]. A digester converts the separated fruits into a paste which is pressed to extract oil. A sludge known as palm oil mill effluent (POME) is produced during this step as a waste product [45]. Pressing the fruits causes the seeds to be trapped in a solid mass of fibers. In a process called depericarping the seeds are removed from these fibers. After the seeds are polished and cracked, the mass of fibers and the shells are sent to be burned, and the kernel is sent to be processed elsewhere [54].

At the kernel processing plant there are two main scenarios [55]. Either power is provided by the oil mill, which is on the same site as the kernel plant, or the plant is powered by electricity from a utility provider. It is more common for the kernel plant to be powered by electricity, and this is the scenario used in the present study. The kernels are pressed in a series of screw presses which extract the oil. The solid portion of the kernel left over, called palm kernel cake, can be used as a fuel or as an animal feed [55]. The crude palm kernel oil is then shipped to a plant to be split and distilled or fractionated into various fatty acids.

Splitting and Distillation

Crude palm kernel oil (CPKO) is a natural fat and as such contains a variety of fatty acids. The typical breakdown of the fatty acids in the fat is shown in Table 4.1. The fatty acids are joined together with a glycerol backbone, and the combined molecule is known as a triglyceride. Splitting is achieved through the reaction shown in Figure 4.2.

To split the triglyceride into individual fatty acids, steam is introduced into the oil along with a catalyst. The heat and water cause the triglyceride to split, producing free fatty acids and glycerol. There are a variety of processes that do this, such as the Twitchell process or the batch autoclave process, but all the different processes essentially work by introduction of steam and catalysts [56]. The processes vary only in how they introduce the steam and in which catalyst they use. Some of the catalysts that may be used are sulfuric acid, sulfonated fatty acids, zinc oxide, calcium oxide

Table 4.1: The fat content of palm kernal oil [49]. The notation used here is number of carbons:number of double bonds.

Fatty acid	Mass percent
Hexanoic acid (6:0)	0.2
Octanoic acid (8:0)	3.3
Decanoic acid (10:0)	3.7
Dodecaonoic acid (12:0)	47
Tetradecanoic acid (14:0)	16.4
Hexadecanoic acid (16:0)	8.1
Fatty acids, total saturated	**81.5**
Oleic acid (18:1)	11.4
Linoleic (18:2)	1.6
Other fats/unknown	3.9

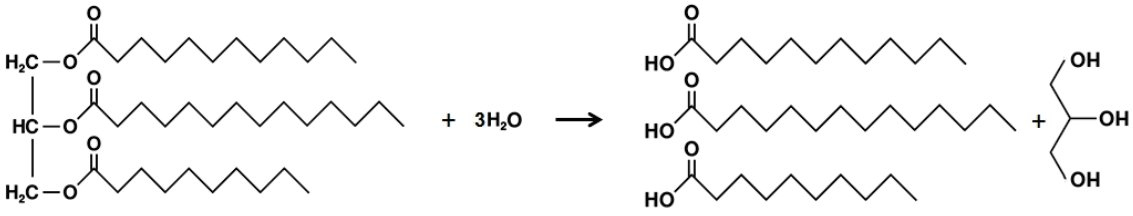

Figure 4.2: The triglyceride is split using water, producing glycerol, and three fatty acid chains.

or magnesium oxide. Since this is technically a reversible reaction, the glycerol must be continuously removed to promote completion of the reaction [56].

Once the oil has been split, it is necessary to separate the varied lengths of fatty acids from each other. This can be done using distillation or fractionation. Distillation is achieved by both heating the crude fatty acids and applying a vacuum. The shorter chain fatty acids evaporate first and are drawn off. This method can purify fatty acids to approximately 98%. Fractionation is a catchall term for many different processes that achieve a higher degree of purity than distillation does [56]. The present study considered distillation as the separation method because 98% is sufficient purity for dodecanoic acid in most solar thermal PCM applications [26]. Distillation produces fatty acids of various chain lengths in different fractions, one of which is the desired end product, dodecanoic acid.

4.2.3 Present Study

Land Use

New palm oil plantations are typically grown on land previously occupied by rainforest or peat. Yee *et al.* [45] quantified the amount of CO_2 released in clearing peat land and replacing it with an oil palm plantation. The CO_2 is quantified per tonne of crude palm oil (CPO) produced [45]. This includes CO_2 from forest conversion, peat decomposition, and emission from fires caused during land clearance. Because the amount of CPO and CPKO produced are proportional, it was possible to relate the amount of CO_2 released to tonnes of CPKO produced. Since only about 10% of oil palm plantations are on peat land, this was factored into the calculations by only including the peat emissions from 10% of the dodecanoic acid produced. The other 90% was assumed to have come from cleared rainforest land. Yee *et al.* also had data for the amount of CO_2 sequestered and released by oil palm plantations and rainforests, which was used to calculate the amount of CO_2 sequestered [45]. The results for this calculation are shown in Table 4.2. Data in the tables may not have proper significant figures, because of rounding, scale, and clarity issues, but the final results all have been treated appropriately for significant figures.

Table 4.2: The amount of CO_2 absorbed and emitted by oil palm plantations. Also included is the CO_2 released by clearing peat land per tonne of crude palm oil (CPO)

Parameter	Amount	Reference
Gross sequestration (tCO_2 ha^{-1} $year^{-1}$)	161	[45]
Total respiration (tCO_2 ha^{-1} $year^{-1}$)	96.5	[45]
Net assimilation (tCO_2 ha^{-1} $year^{-1}$)	64.5	[45]
Peat land emissions (tCO_2 $tCPO^{-1}$)	1.70	[45]
Weighted peat land emissions (tCO_2 $tCPO^{-1}$)	0.166	Present study

Table 4.3: Data for energy and CO_2 in fresh fruit bunch (FFB) production.

Parameter	Amount	Reference
FFB yield (tFFB ha^{-1} $year^{-1}$)	20	[52]
N fertilizer use (kgN $tFFB^{-1}$)	3.65	[52]
Equivalent CO_2 emissions for other fertilizers ($kgCO_2$ $tFFB^{-1}$)	14.6	[52]
N_2O emissions (kgN_2O $tFFB^{-1}$)	0.0365	[52]
CO_2 equivalent for N_2O ($kgCO_2$ $tFFB^{-1}$)	10.8	[52]
Diesel consumption (GJ $tFFB^{-1}$)	0.16	[52]
Embodied energy of N fertilizer (GJ tN^{-1})	56.86	[57]
Embodied energy of fertilizer used (MJ $tFFB^{-1}$)	207.5	Present study
Total CO_2 (kg CO_2 $tFFB^{-1}$)	67.32	Present study
Total Energy (MJ $tFFB^{-1}$)	367.54	Present study
CO_2 equivalent for N_2O (kg $tFFB^{-1}$)	10.8	Present study

Fresh Fruit Bunch Production

The major inputs into this part of the LCA were nitrogen, phosphorus and potassium fertilizers. Inputs and outputs for the process are shown in Table 4.3. As can be seen from Table 4.3, the fertilizer consumes the majority of the energy for FFB production. Of the 367 MJ $tFFB^{-1}$ 208 MJ $tFFB^{-1}$ or 57% are from fertilizer contributions.

Milling

The major co-product is crude palm oil. See Tables 4.4 and 4.5 for detailed information. Conversions for fuel and transport to energy and CO_2 emissions were taken

Table 4.4: Energy and CO_2 for extracting kernels and 1 t crude palm oil (CPO) [54, 58]

Parameter	Amount
FFB (t)	3.10
Power from turbine (MJ)	224.08
Power consumption from grid (MJ)	1.76
Diesel consumption for mill (MJ)	100.33
Transportation of diesel to mill (t km)	0.54
Kernels (t)	0.41
Shells (t)	0.23
Empty fruit bunches (t)	0.71
POME (t)	1.86
CO_2 from POME pond (kg)	36.04
Flue gas(CO_2) (kg)	41.28
Total energy (MJ $tCPO^{-1}$)	326.66
Total CO_2 (kg $tCPO^{-1}$)	588.18

from Ashby [58]. Because of burning of the oil palm husks, a large amount of fuel is saved during extraction of CPO. 224 MJ $tCPO^{-1}$ or 69% of the 327 MJ $tCPO^{-1}$ total needed to produce CPO and extract the palm kernels. The power savings can also be applied to the extraction of CPKO as can be seen in Table 4.5. If the CPKO extraction plant is located on site with the CPO plant, significantly less electricity is used (449 MJ $tCPKO^{-1}$ vs 44 MJ $tCPKO^{-1}$). However, this arrangement is not typical, and as discussed later, in this study the CPKO extraction plant was assumed to be located far from the CPO plant.

Splitting and Distillation

An information brochure from Lurgi, a well known manufacturer of fatty acid treatment plants, lists the average utility usage of splitting and distilling plants [59]. Table 4.6 has detailed numbers. Major co-products for this phase are glycerol and other fatty acids.

The inputs and outputs of all the previous steps were integrated, and the energy required to produce a given amount of dodecanoic acid was calculated. The amount of CO_2 emitted was also calculated using similar steps. For all usages of electricity

Table 4.5: Energy and CO_2 for extracting 1 t crude palm kernel oil (CPKO) from palm kernels [55]. When palm kernel presses are located near to palm oil processing plants, energy from burning byproducts can be used to power palm kernel oil extraction processes.

Parameter	**CPKO located far away from palm oil plant**	**CPKO with palm oil power**
Palm kernels (t)	1.07	1.07
Electricity from grid (MJ)	448.6	44.0
Transportation of kernels (t km)	149.4	2.24
Palm kernel cake (t)	1.12	1.12
Transport energy (MJ)	134.5	2.016
Transport CO_2 (kg)	16.4	.246
Total Energy (MJ $tCPKO^{-1}$)	583.1	46.0
Total CO_2 (kg $tCPKO^{-1}$)	254.2	23.46

Table 4.6: Required utilities for splitting 1 t crude oil [59].

Parameter	**Fatty acid splitting**	**Fatty acid distillation**
Plant capacity (t day^{-1})	40-400	50-200
Heating steam (at 60 bar, 270 °C) (kg)	160	370
Steam (at 3-10 bar) (kg)	N/A	150
Cooling water (m^3)	12	15
Electrical energy (MJ)	10	5
Process water (m^3)	0.6	N/A
Export Steam (at 3 bar) (kg)	N/A	120
Energy water to steam(25-270 C) (MJ)	90	292.5
Energy to pressurize steam (MJ m^{-3})	245.7	285.8
Total energy (MJ)	2583	3169
Total CO_2 (kg)	380.22	466.41
Total water use (kg)	12760	15640

during dodecanoic acid manufacture, the amount of CO_2 emissions was calculated assuming a standard mix of Malaysian power, which mostly consists of natural gas and hydroelectric power [45].

4.3 System

Since PCMs have not been commercially implemented as a thermal energy storage (TES) medium in a solar powered hot water system, there is significant estimation involved in the following calculations. A basic solar TES system could consist of two storage tanks, (*i.e.* a water heater and an insulated PCM tank), a solar collector, an electric heater, piping, pumps, PCM, instrumentation, and controllers. This study neglected the instrumentation and controllers since they contribute much less to the quantities under study than the other parts do. Solar collectors take one of two common forms, either the flat plate form or evacuated tubes. Both types were modeled in the present study, their areas being 4.0 m^2 and 2.4 m^2 for the flat plate and the evacuated tube respectively. These sizes were chosen by Hang *et al.*, who determined that they would have similar capital costs [60]. The evacuated tube collector is more expensive, but has less heat loss and therefore can achieve a higher temperature increasing efficiency. Therefore, despite the different size of the collectors a similar amount of heat can be absorbed. Tables 4.7 and 4.8 present the detailed material inventories. The bill of materials needed for the panels came from the work of Hang *et al.* [60], but energy and CO_2 values were calculated in the present study with data from Ashby [58]. Myrans calculated the embodied energy and CO_2 emissions of the insulated storage tanks (160 L) [61], which was 4020 MJ and 95 kg of CO_2 per tank. The electric heater is needed in case the solar energy is insufficient to provide enough hot water and was modeled as a simple element containing 1.58 kg of nichrome. For the piping, 3.0 kg of copper, which gives between three and six meters of piping depending on the size, was assumed to be sufficient for the application.

The calculation for the phase where the product is used is much harder to quantify as the system boundaries are extremely complex. The temperature of the heat transfer fluid, the ambient temperature, and the heat transfer characteristics of the PCM all can have dramatic effects on the calculation. However, some LCAs have been carried out comparing solar thermal to conventional water heating with positive results for the

Table 4.7: Material inventory of 4.0 m^2 flat plate collector [58, 60].

Component	Material	Amount	Units	Embodied Energy (MJ $unit^{-1}$)	CO_2 produced (kg $unit^{-1}$)	Embodied energy (MJ)	CO_2 produced (kg)
Trim	Aluminum	1.80	kg	215	12.2	387	21.9
Absorber	Copper	2.82	kg	60.0	3.86	169	10.9
Frame	Stainless Steel	4.14	kg	92.7	5.55	384	23.0
Insulation	Rock wool	2.43	kg	30.3		73.6	
Insulation	Corrugated board	3.68	kg	52.0	1.17	191	4.31
Glazing	Glass	9.12	kg	19.2	1.45	175	13.2
Transfer fluid	Propylene glycol	1.01	kg	73.0		73.7	
Sheet	Copper	2.82	kg	60	3.86	169	10.9
Production	Electricity	1.16	kWhr	3.6	0.50	4.18	0.58
					Total	**1626.5**	**84.79**

Table 4.8: Material inventory of 2.4 m^2 evacuated tube collector [58, 60].

Component	Material	Amount	units	Embodied Energy (MJ $unit^{-1}$)	CO_2 produced (kg $unit^{-1}$)	Embodied energy (MJ)	CO_2 produced (kg)
Absorber	Copper	2.8	kg	60	3.86	168	10.8
Frame	Stainless steel	4.0	kg	92.7	5.55	371	22.2
Insulation	Rock wool	2.03	kg	30.3		61.5	
Insulation	Corrugated board	3.33	kg	52	1.17	173	3.90
Glass tube	Glass	14.2	kg	37.4	2.37	531	33.8
Transfer fluid	Propylene glycol	0.654	kg	73.0		47.7	
Sheet	Copper	2.8	kg	60	3.86	168	10.8
Production	Electricity	17.0	kWhr	3.6	0.5	61.2	8.5
Production	Natural gas	16.5	MJ	1.0	.055	16.5	.908
					Total	**1597.9**	**90.9**

solar thermal systems [60, 62, 63]. These are typically done using modeling software such as TRNSYS that can effectively model the system boundaries. However, there do not seem to be any published studies using PCMs, largely because in many cases water is an adequate heat storage medium. The advantages of using a PCM are subtle and may not apply in many circumstances. A PCM has a higher storage density than water and therefore could be used in a more limited space. While an extensive modeling using a program like TRNSYS would be quite useful, it is beyond the scope of this thesis. Therefore a smaller and simpler task, setting upper and lower bounds for how much energy a PCM system could save compared to a typical water heating system, was undertaken.

The functional unit of the LCA the amount of hot water at 60 °C needed by a typical US family for one day (237 L) [60]. Several scenarios were set up to mimic lower and upper bounds of the problem. The best case scenario, called BEST, is that the PCM has sufficient heat to supply the household with all its hot water needs, and the electric heater is never needed. The absolute worst case is that there is no solar energy coming in and the heater must supply all of the hot water. However, this is nonsensical because even in the middle of winter there is still some solar radiation. Instead, a low case, called WORST, was set up where the PCM was able to provide hot water at 43.3 ℃ (dodecanoic acids melting point) half the time and then unable to provide any hot water the rest of the time. A more reasonable estimate, called INTERMEDIATE, was also considered. In this scenario the PCM heated the water to 43.3 ℃ all of the time and the electric heater heating the water the final 18.7 degrees. A municipal inlet temperature of 15 ℃ was assumed. Using a higher or lower inlet temperature would slightly decrease or increase, respectively, the amount of energy needed to heat the water.

4.3.1 Lifetime and disposal

When no longer functioning as a phase change material, dodecanoic acid could be disposed of in two ways. It could be added to biodiesel feedstock to be used as a fuel. This would release the carbon into the atmosphere, but liberate the energy contained within. Or disposing the dodecanoic acid in a landfill would sequester the carbon for many years, although the embodied energy would be lost. The solar thermal

system could be recycled or disposed of in a landfill, as is more appropriate for the components. The system is expected to last at least 10 years, and may last twice as long with regular maintenance [64].

4.4 Analysis of Results

Manufacture

The CO_2 emissions in the manufacture phase for dodecanoic acid are outweighed strongly by the carbon sequestration by the plantation, yielding a net negative result, meaning net CO_2 absorption, -67.8 tonnes of CO_2 per kg of dodecanoic acid, as can be seen in Figure 4.3. However, since many plantations replace rainforests, this cannot necessarily be counted on being a true carbon sink. Therefore, for future calculations, this contribution was neglected, as rainforests and oil palm plantations sequester close to the same amount of CO_2 [45], to give the positive value of 1.71 tonnes CO_2 per kg of dodecanoic acid. If the plantation sequestration is neglected, the peat land emissions, and the fresh fruit bunch production dominate as shown in Figure 4.4.

The embodied energy of the dodecanoic acid is 12300 MJ t^{-1}. As shown in Figure 4.5 , the production of the FFB is the largest factor in the production of dodecanoic acid accounting for two thirds of the total energy.

For both solar collectors investigated here, the evacuated tube and the flat plate, the embodied energies are almost the same. The amount of dodecanoic acid used was 164 kg, which was calculated to be sufficient to store the energy coming from a solar collector of the size in the present study. The default electrical water heating system without solar panels or dodecanoic acid has about a third of the embodied energy of the others as can be observed from Figure 4.6. Note that the embodied energy of the storage tanks dominates over the other components. This is because of the large amount of steel present in storage tanks, and also because of the need for two tanks in solar thermal systems utilizing PCMs. Figure 4.7 shows that the pattern for CO_2 emissions is nearly the same for the flat plate, evacuated tube and electric hot water heater.

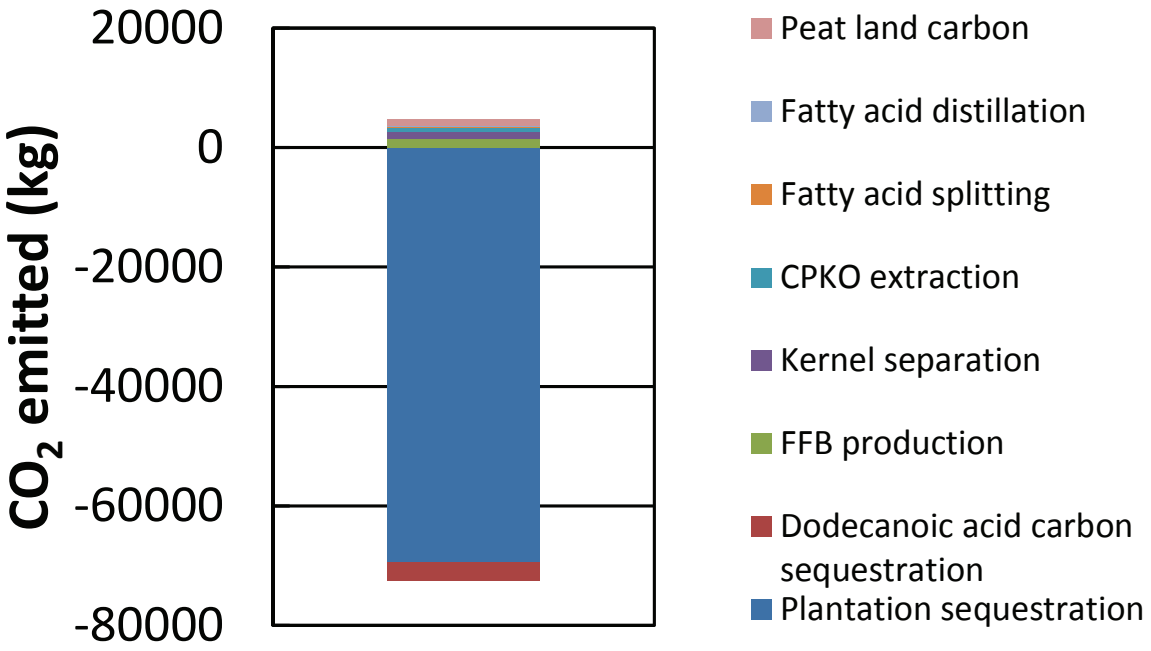

Figure 4.3: CO_2 emissions and absorptions during production of one tonne of dodecanoic acid showing large effect of the plantation sequestration on CO_2 uptake. Plantation sequestration is the amount of CO_2 held by the trees in a plantation in the form of wood, leaves, and other vegetable matter,

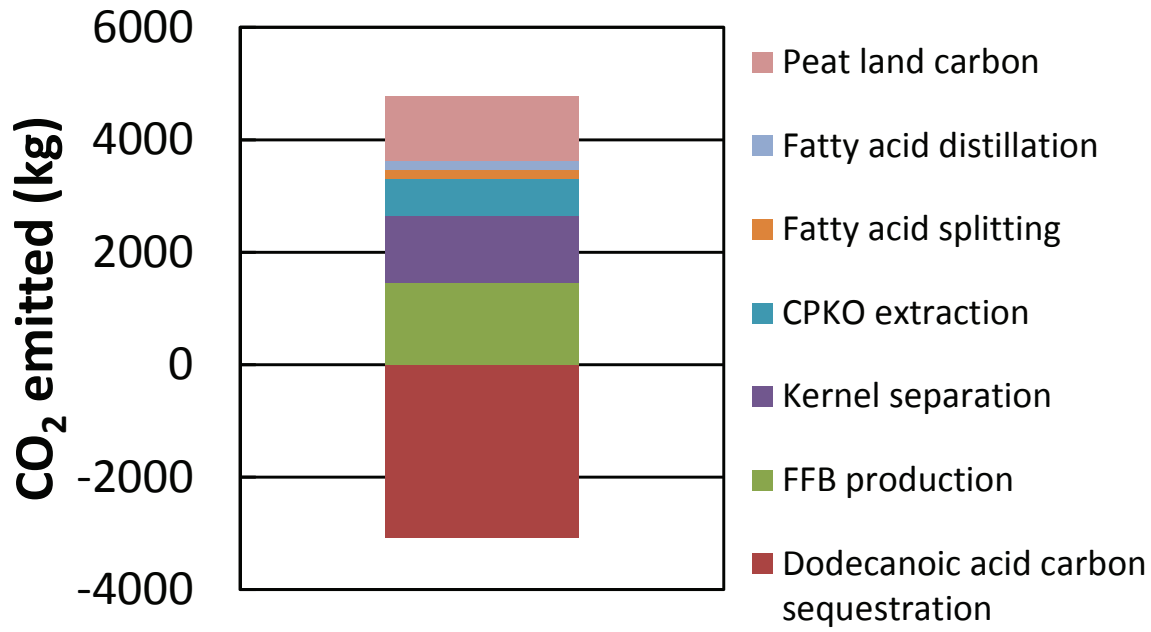

Figure 4.4: A closer look at the CO_2 emissions for the production of one tonne of dodecanoic acid, neglecting the effect of the oil palm plantations' uptake of CO_2.

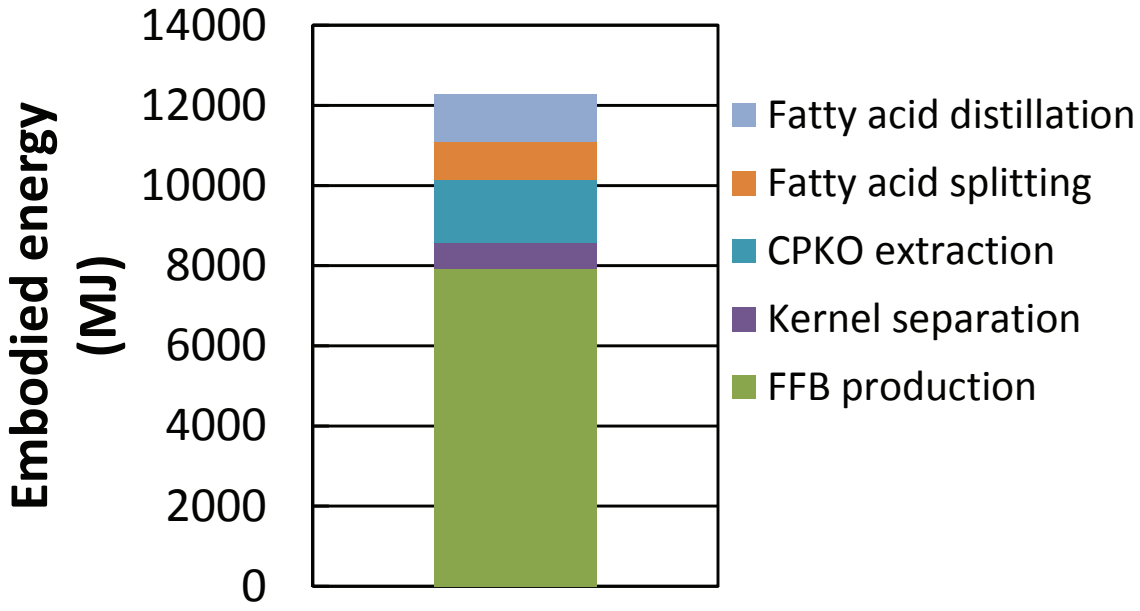

Figure 4.5: Embodied energy for the production of one tonne of dodecanoic acid broken down into separate processing steps.

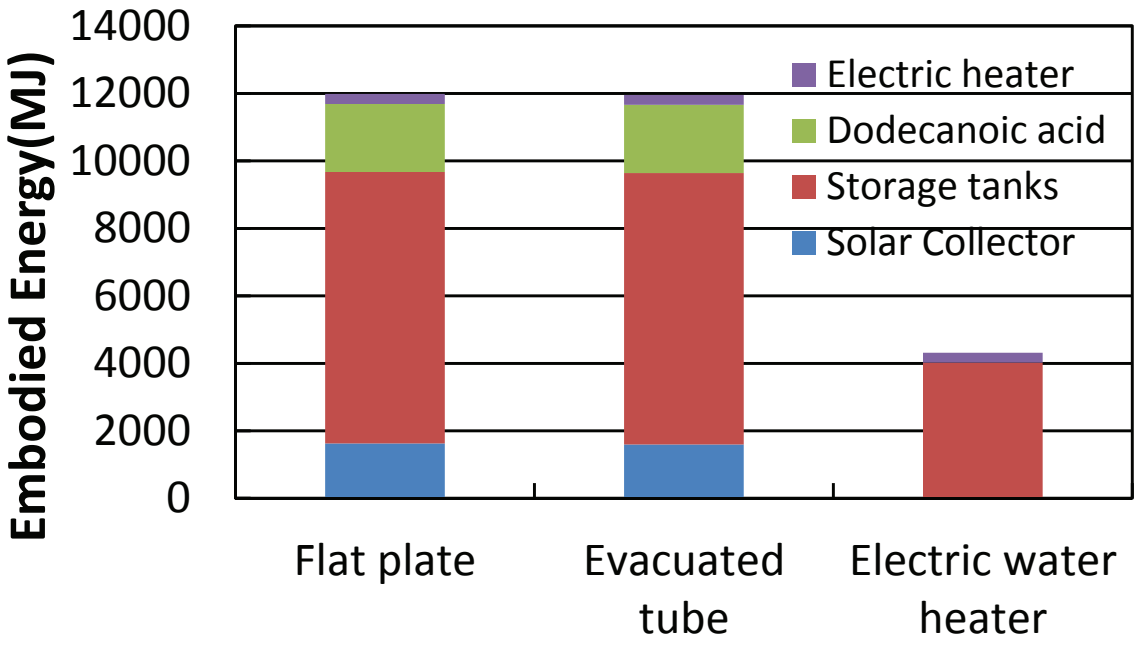

Figure 4.6: Comparison of the embodied energy of a variety of solar thermal systems.

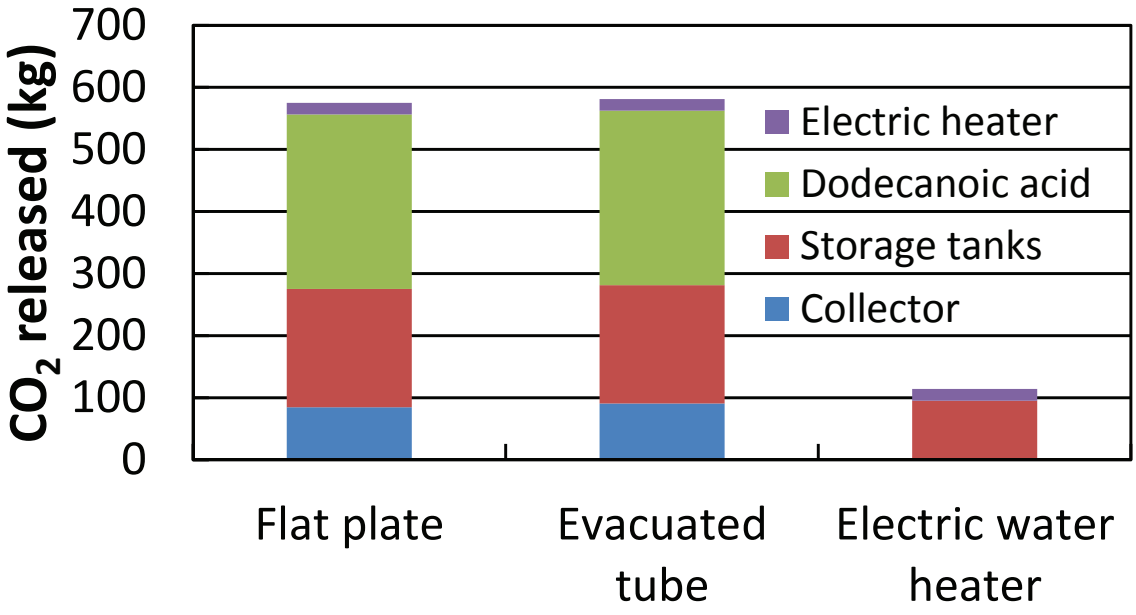

Figure 4.7: Comparison of CO_2 emissions for production of different domestic hot water systems.

Use

Following the scenarios set up previously, the payback time for the embodied energy of the system can be established. Because the embodied energies were nearly the same for flat plate and evacuated tube collectors, all scenarios presented here used the flat plate for ease of understanding. All of the scenarios pay off with respect to a typical water heater in less than two years as demonstrated in Figure 4.8. With the expected life of the system at more than 10 years this is a very reasonable payback time. About 154 GJ and 100 GJ for WORST and INTERMEDIATE respectively are expected to be saved over the course of 10 years. The CO_2 payback time (without the effects of the forest sequestration) is even faster. Even for the worst case scenario it is less than a year as shown in Figure 4.9. For WORST, over the course of ten years, the system will save about 6.61 tonnes of CO_2 compared to a typical electric water heater. For INTERMEDIATE, the system saves about 13.7 tonnes of CO_2. This takes into account the initial higher emissions of the solar thermal system. Implementing a solar thermal PCM system would prevent the release of CO_2, over ten years, roughly equivalent to the annual emissions of between 1.4 and 2.9 average passenger vehicles

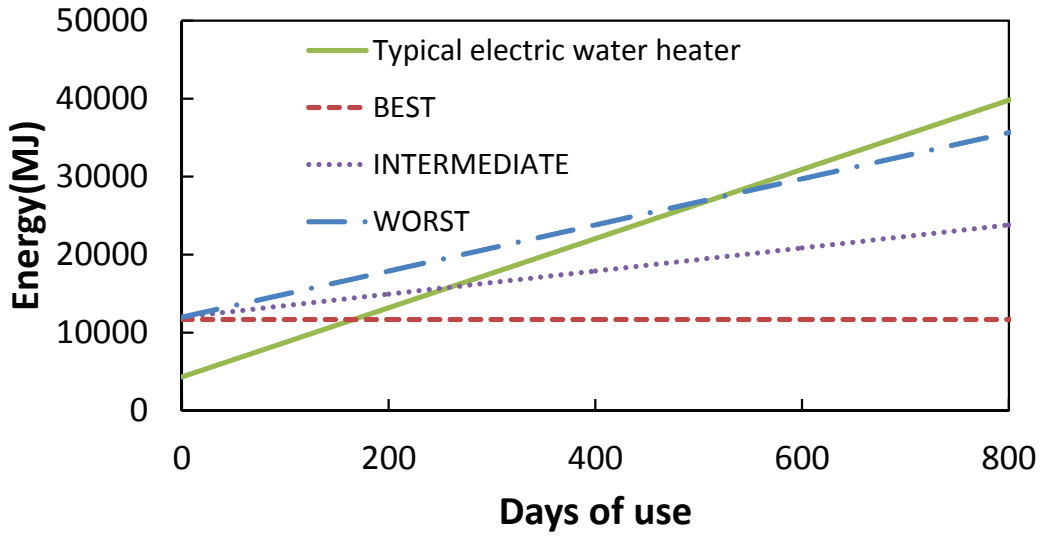

Figure 4.8: Time required to break-even for embodied energy in several scenarios of a flat-plate solar thermal PCM water heater. BEST uses no additional electric heater, INTERMEDIATE uses an electric heater for half its energy requirements above 43.3℃, and WORST uses a heater for all its energy requirements above 43.3℃. The point at which the typical electric water heater line crosses each of the others is the breakeven point for that scenario.

[65].

From an economic perspective the numbers are not as promising. Complete solar thermal systems are expensive, costing around $5000 [64] and the savings are not spectacular. Thermo Dynamics Ltd. claims that costs of water heating are reduced about 65% on average [64]. According to the water usage plan outlined previously [60], and assuming that standard Nova Scotia Power electric rates apply [66], an average family can expect to spend approximately $600 a year on water heating. A 65% reduction means that about $390 can be saved every year (which is what the Themo Dynamics Ltd. website lists as potential savings as well [64]). This means it takes about 10 years to recover the cost of the initial investment. This is as long as the warranty from Thermo Dynamics Ltd. lasts, but the system is likely to last longer, although some maintenance may be required. The expected savings of the system over its lifetime barely covers the initial cost of the system. Adding the cost of the PCM only causes the outlook to be bleaker. As demonstrated in Figure 4.10, the cost of the various scenarios fall above and below the expected value from Thermo Dynamics

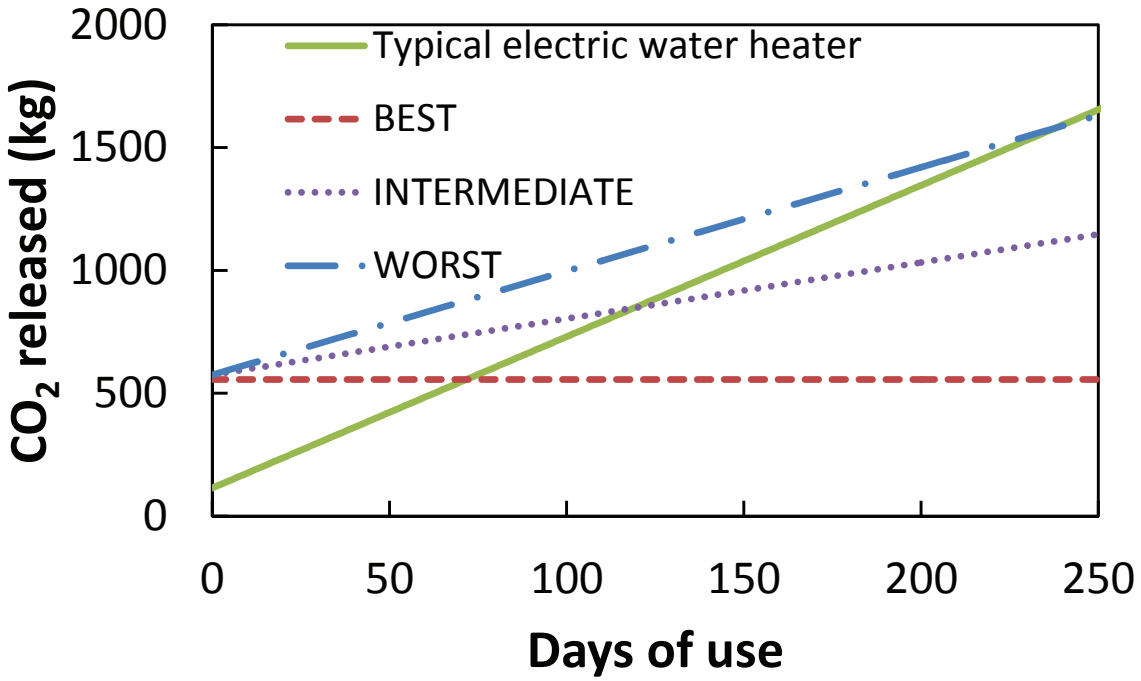

Figure 4.9: Payback time with respect to CO_2 emissions for several scenarios of flat-plate solar thermal PCM water heater. BEST uses no additional electric heater, INTERMEDIATE uses an electric heater for half its energy requirements above 43.3℃, and WORST uses a heater for all its energy requirements above 43.3℃ . The point at which the typical electric water heater line crosses each of the others is the breakeven point for that scenario.

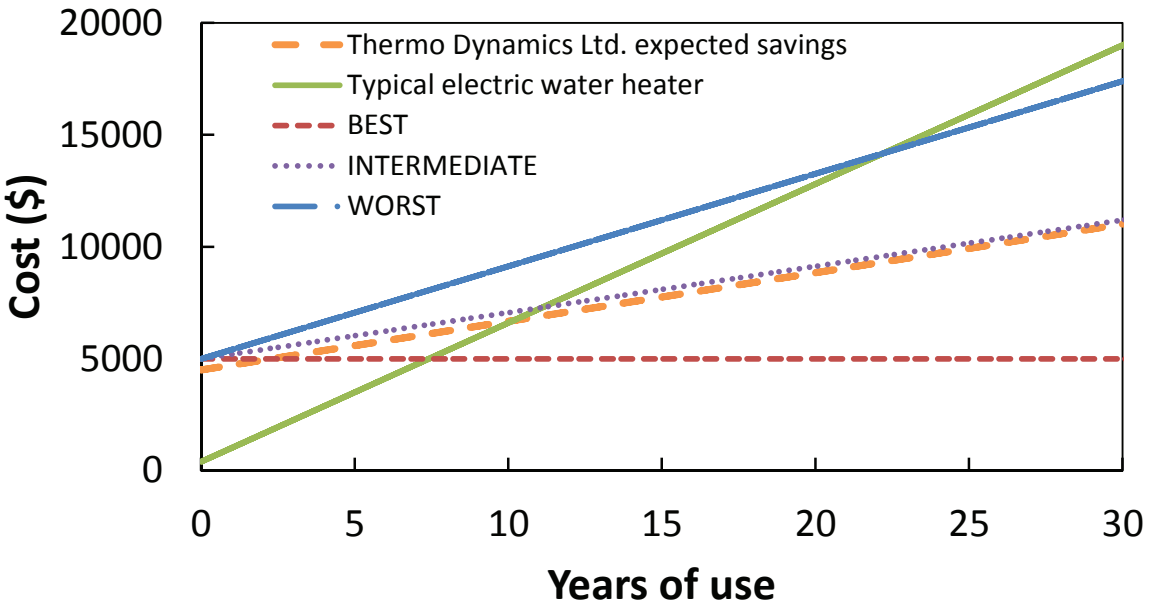

Figure 4.10: Time required to break-even for cost in a flat-plate solar thermal PCM water heater. BEST uses no additional electric heater, INTERMEDIATE uses an electric heater for half its energy requirements above 43.3 °C and WORST uses a heater for all its energy requirements above 43.3 °C. Thermo Dynamics Ltd. expected savings depicts the expected savings from having a Thermo Dynamics solar thermal energy storage system installed. The point at which the typical electric water heater line crosses each of the others is the breakeven point for that scenario.

Ltd. INTERMEDIATE closely mirrors the expected savings that Thermo Dynamics Ltd. projects, which lends credence to the idea that INTERMEDIATE is a good approximation for an actual solar thermal storage system. With such slim savings it is unlikely that many people will be inclined to invest in such a system, without additional economic incentives. There are some governments that have started doing so. For example, in Halifax, there is the Solar City program, where the Halifax Regional Municipality finances the initial cost of a solar thermal hot water system by providing a loan [67].

The land use is another important consideration. The annual production of one hectare of a oil palm plantation is about one tonne of dodecanoic acid. This means that it takes 0.144 hectare, or a square of about 38 m on each side, to produce enough dodecanoic acid in a year for one solar thermal system. But since that plantation produces that much every year and the lifetime of a solar thermal energy storage is

at least ten years, it could be argued that only 0.0144 hectares, or a square of 3.8 m on each side, are needed. It should not be forgotten that this area is also producing many other coproducts, such as palm oil, glycerol, and other fatty acids.

Overall, the picture for dodecanoic acid as a PCM storage material is promising with some caveats. In terms of embodied energy and CO_2 emissions, dodecanoic acid has a relatively quick payback time, although economically it is slow to pay back. Before becoming too optimistic, however, one must address the drawbacks. Most importantly the environmental and conservation concerns are not to be dismissed. Deforestation releases huge amounts of CO_2 and although palm oil plantations can slowly replace that effect, there are some inherent problems with monoculture [68]. Oil palm plantations have also been repeatedly accused of causing large amounts of deforestation that affects endangered species such as the orangutan [69]. These issues are too complicated to explore at great depth in this thesis. Suffice it to say that whenever a source for dodecanoic acid is selected, care should be taken to choose only plantations or companies that are committed to safe environmental practices. There are some organizations in place, *e.g.* the Roundtable on Sustainable Palm Oil [70], to provide guidelines for companies to follow and to guide consumers.

Chapter 5

Solar Thermal Energy Storage with Dodecanoic Acid

5.1 Introduction

As part of the requirements for DREAMS, an internship at Nova Scotia Community College (NSCC) in Dartmouth, Nova Scotia was undertaken. The goal of this project was to design and build a solar thermal energy storage system that could be used as a testbed for future projects and experiments to build on. Preliminary measurements were also taken to verify the effectiveness of the energy storage system.

5.2 Description and Specifications

The solar thermal system was designed to be relatively simple. It has two plumbing lines which exchange heat with a PCM tank. One line, the "hot" (glycol) line, collects heat from the sun and deposits heat in the PCM, and the other line, the "cold" (water) line, takes heat from the PCM and transfers it to someplace useful, be it a fan and coil space heater, or a hot water tank. The glycol loop used a 60/40 propylene glycol/water mixture by volume as a heat transfer fluid.

The PCM storage consisted of the bottom half of a commercial 150 L water heater tank. Aviation snips were used to remove the outer sheet metal shell. The insulation was removed in a small band, and then an angle grinder was used to cut the internal tank in two. The maximum depth of the selected half was 52 cm and the internal diameter was 46 cm. An insulating cap was made of expanded polystyrene wall insulation and fitted to the tank. Holes were drilled in the cap to allow heat exchanger tubes and thermal probes to pass through.

The plumbing lines for both water and glycol were mostly 1/2 NPT brass pipe. The lines were equipped with visual (analog) and digital flow meters, and thermocouples. A schematic of the system can be seen in Figure 5.1. Other features necessary for smooth functioning of a thermal transfer fluid system, such as relief valves and

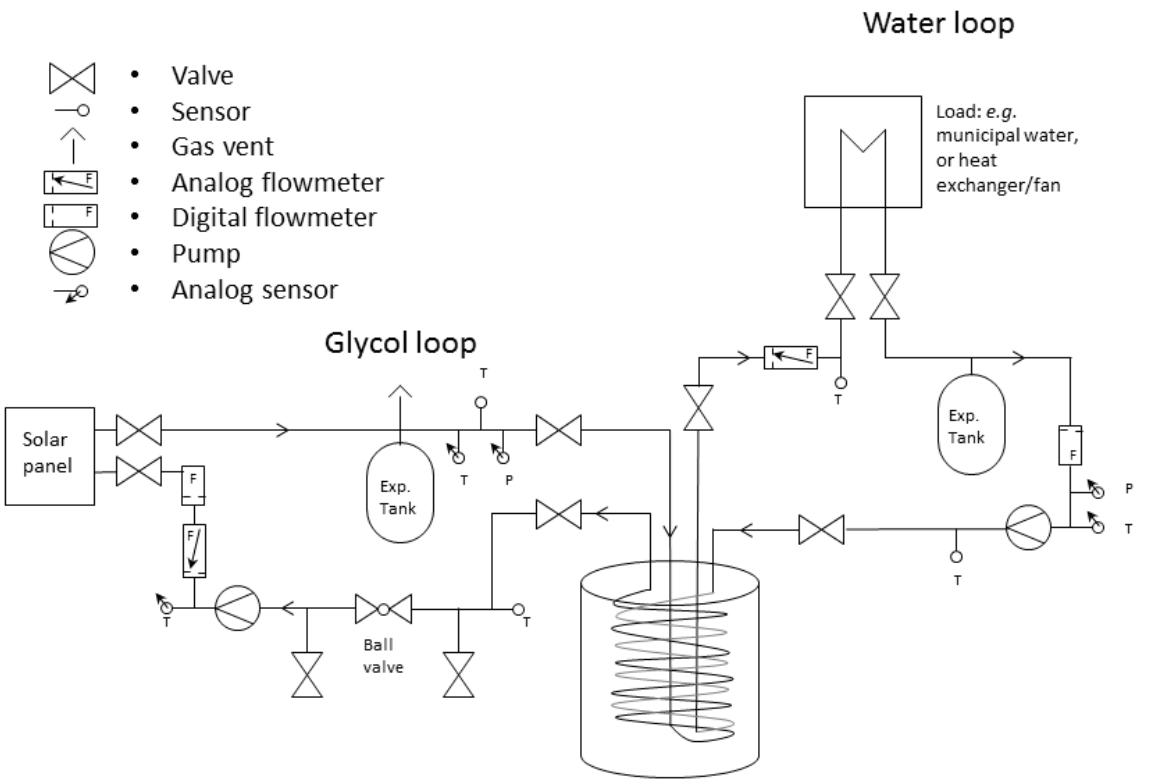

Figure 5.1: A schematic drawing of the plumbing of the PCM solar thermal storage system The heat exchanger was valved off so that different heat exchangers could be put on the system with ease. No load was used during the preliminary measurements presented here.

expansion tanks (Watts Regulator ETX-15 and Bell & Grove HFT-15 for water loop and glycol loop respectively), were also present.

The heat exchanger was made of 1/4" (0.635 cm) diameter copper tubing coiled into two concentric helices. Each helix was about 450 cm long and consisted of helices 32 cm in diameter with a pitch, *i.e* distance between spirals, of 10 cm, and with four turns. Since the helices were coaxial and the tubes had a finite diameter, there was a distance of about 4.4 cm between the pipes. At the bottom of the spirals the tubes were directed to the central axis of the helices and were brought up the center axis and out of the tank. At the top of the helices the tubes left the tank at a point along the circumference. Figure 5.2 shows a photograph of the coils before insertion into the tank. The circumferences of the helices were set by making the volume inside them approximately the same as the volume outside the helices.

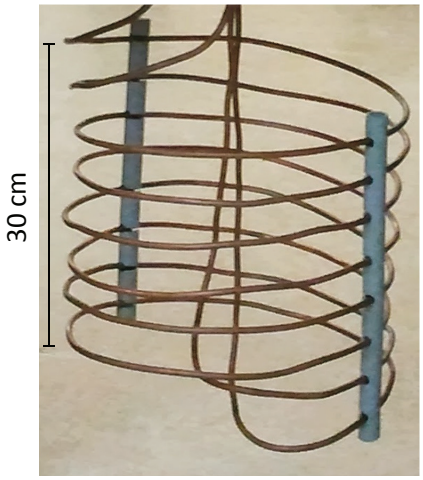

Figure 5.2: A photograph of the heat exchanger coils. PVC spacers hold the coils at a fixed pitch. Note that there are two separate tubes arranged coaxially.

Twelve thermocouples were positioned around the tank as shown in Figure 5.3. There were three radial positions and four depth positions. Each radial position had four depths and was spaced 90° from its neighbors. The radial positions were designated starting from the center of the tank and moving towards the edge and are specified here as inner, mid, and outer. Each of the inner probes was spaced 2 cm from the point located midway between the two central heat exchanger tubes. As one of the tubes is located in the exact radial center of the tank, the inner probes were not exactly centrally located. The mid probes were equidistant between the center and the edge and the outer probes were 2 cm from the edge. The depth positions were designated using numbers from 1 (shallowest) to 4 (deepest). The bottom of the tank was curved upward like a dome so the longest thermocouples were uneven lengths. The shallowest probes were all the same length (20.3 cm), and the longest probes all left a gap of about 5 cm from the bottom. This meant the longest probe was 53.3 cm in the outer row, 50.8 cm in the middle row, and 48.3 cm in the inner row. The remaining lengths were evenly spaced between the two extremes for each row. The middle positions were offset from the outer and inner by 45° to maximize the space between the probes. The positioning was set this way to attempt to determine an average estimation of the system as a whole, although because of the non-symmetrical arrangement of the coils this was problematic.

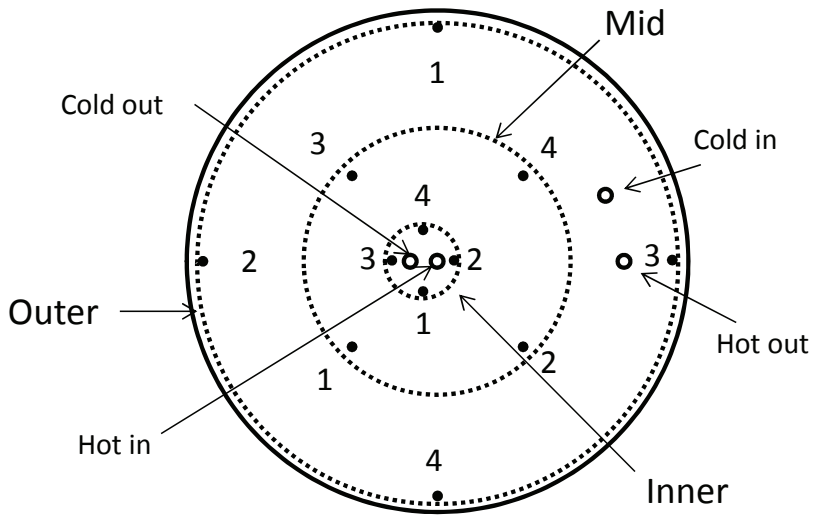

Figure 5.3: A top-down diagram showing how the thermocouple probes are arranged. The numeral 1 represents the shallowest thermocouple and the 4 represents the deepest. Inner, mid and outer rows are also shown. Relative positions of inlets and outlets of the heat exchanger tubes are shown as well. The inner row is slightly offset from the center due to the heat exchanger pipe coming directly out of the center.

Four thermal probes were also situated in the thermal transfer loops as the loops come out of the tank. This gave inlet and outlet temperatures for both the cold and hot lines.

All thermal probes were T type, copper-constantan, thermocouples housed in stainless steel sheaths of 1/16" in diameter in the tank and 1/8" in the thermal transfer fluid lines. A National Instruments NI-cDAQ-9174 compactDAQ with the modules, NI 9213, NI 9211, and NI 9201 was used to record data.

Solar irradiance was measured using an Apogee sp-215 at simultaneous intervals with the temperature measurements, *i.e.* once a minute for 24 hours a day.

Dodecanoic acid (Alfa-Aesar, 98%) was chosen as the phase change material. It has been found to have most of the required characteristics for a good phase change material, a relatively high melting enthalpy (184 kJ kg^{-1}), a long cycle life (>500 cycles), and a small degree of supercooling (*ca.* 2 ℃) [26]. The major drawback with dodecanoic acid is its low thermal conductivity (0.150 W m^{-1} K^{-1}) [26] compared to metals (*ca.* 100 W m^{-1} K^{-1}) or salt hydrates (*ca.* 0.3 W m^{-1} K^{-1}) . However, its benefits well outweigh its drawbacks. A mass of 60 kg of dodecanoic acid was added

to the storage tank by melting about 8 kg at a time and pouring the liquid through a hole in the cap.

The solar thermal system was sized for a 2.982 m^2 solar panel. The actual panel used was a Model G32-P solar collector from Thermo Dynamics Ltd. [64] The approximate amount of energy per day, on average, that a panel of that size could absorb and feasibly transfer to another material was calculated. The amount of energy available from the sun each day varies greatly from month to month due to seasonal and climatic variations. Thus the average value was used. The amount of dodecanoic acid that was needed to store that much energy daily was then calculated and determined to be about 70 kg. The actual amount used was 60 kg of dodecanoic acid as this would fit into the modified water heater tank. The solar panel was located in a relatively sunny spot with southern exposure. However, it was shaded by buildings in the morning and evening, which resulted in sharp drops of light intensity during those periods. Since it is expected that every day part of the sunlight would get blocked, 60 kg seemed quite adequate for the system.

5.3 Preliminary Measurements

Some preliminary measurements were taken to establish that this system could be used as a research bed for a variety of experiments, such as testing different heat exchangers, evaluating under different seasonal conditions, and testing a variety of charging and discharging regimes. For these preliminary measurements the system was allowed to cool to ambient temperature, and then at the start of solar collection the pump was turned on. The system collected energy until sunset, and the temperature was continually monitored using all the temperature probes. No load was put on the system; the system was allowed to charge without any forced heat loss. This measurement assessed the amount of heat the system could absorb given an input of energy. Several sunny and partly cloudy fall days were measured in this way as comparisons.

To determine the amount of power the PCM (neglecting the walls of the tank, temperature probes, and heat exchanger pipes) was absorbing at a given temperature measurement, the following equation was applied:

$$Power = (T_{inlet} - T_{outlet})C_{p,htf}(T_{ave})\rho_{htf}(T_{ave})A_{pipe}v \tag{5.1}$$

where T_{inlet} is the temperature of the glycol loop before traveling through the tank, T_{outlet} is the temperature of the glycol loop after traveling through the tank, $C_{p,htf}(T_{ave})$ is the heat capacity of the heat transfer fluid at the average temperature of T_{inlet} and T_{outlet}, $\rho_{htf}(T_{ave})$ is the density of the heat transfer fluid at the average temperature, A_{pipe} is the cross sectional area of the fluid in the pipe, and v is the velocity of the fluid through the heat exchanger pipe. The terms $A_{pipe}v$ together represent the volumetric flow rate, which was measured directly using a rotational flow meter.To get the amount of energy absorbed this power value was then multiplied by the amount of time between each measurement, which was 60 seconds in all experiments using this system. An energy versus time graph was created by summing every energy up to a given time. Although more measurements were available, only energy lost or gained while the pump was operating was considered.

The amount of energy the collector had absorbed was determined by,

$$Energy = (ItA_{collector}a) \tag{5.2}$$

where I is the solar irradiance at a certain time, t is the measurement interval, $A_{collector}$ is the area of the collector, and a is the absorptivity of the material. Relevant collector specifications were acquired from Thermo Dynamics Ltd. [64] Equation 5.2 merely accounts for the energy from solar radiation that the collector absorbs and does not account for any heat losses the collector may experience.

5.4 Results

Four days were selected (October 5, 10, 19, and 26, all in 2013) as representative of the desired type of day for solar thermal applications. The conditions of the days were as follows: The dodecanoic acid was at equilibrium at *ca.* 20 ℃ and fully solidified at the start of the day, and the day was sunny. The solar irradiance (W m^{-2}) versus time graphs for each day are shown in Figure 5.4.

Figure 5.5 represents the raw data for tank temperatures with the glycol inlet temperature included for comparison. It is interesting that on each day one or more probes on the top layer, *i.e* "1", experienced a sudden increase in temperature. Perhaps some liquid trapped below escaped upward and caused a rapid heating in the vicinity of one of those probes, and this is why the effect seems random in magnitude

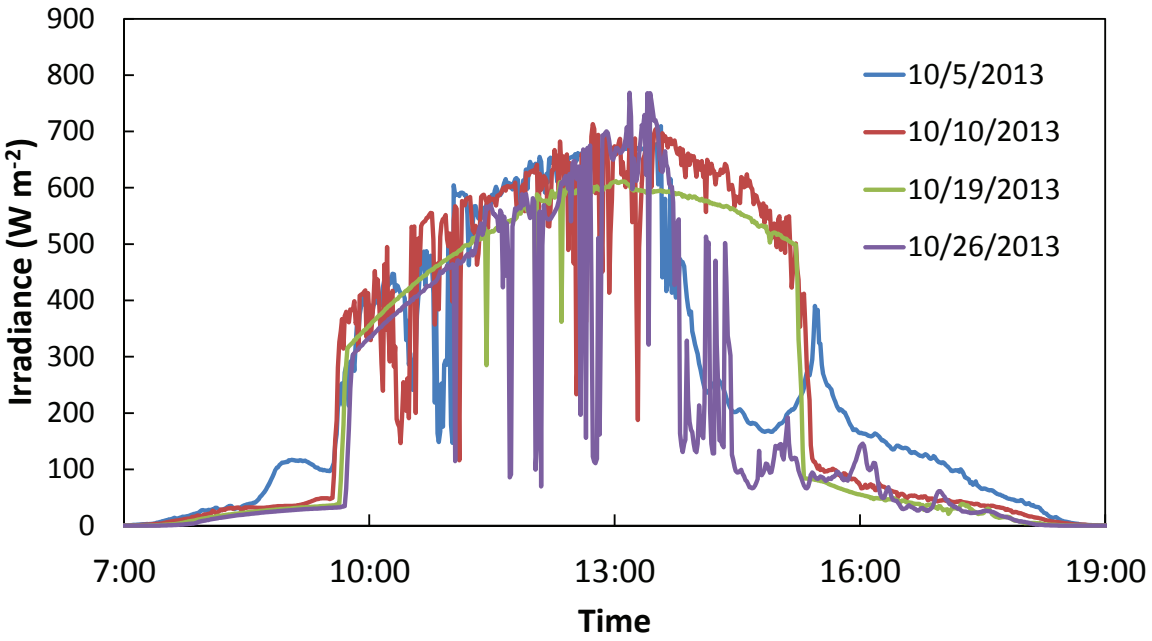

Figure 5.4: A graphical representation of the solar irradiance for four days in October of 2013.

and position. Outer3 and Inner2 are notable because every day they rose in temperature much more quickly than the other probes. This was because they were located close to the glycol pipe, as can be seen in Figure 5.3, and therefore experienced the heat sooner than the other probes. Outer3 and Inner2 were in the vicinity of liquid PCM as can be construed by the fact that their temperatures exceeded the melting point of dodecanoic acid (43.3 ℃). October 10 is remarkable in that several probes other than Outer3 and Inner2 were also in the vicinity of liquid dodecanoic acid. On October 26 the pump started before the heat transfer fluid had had a chance to absorb solar radiation, and the system lost heat to the environment at about 09:30.

Figure 5.6 represents averaged tank temperature data with total energy absorbed superimposed so that the system as a whole can be visualized. On all four days when the heat transfer fluid stopped receiving energy from the sun, its temperature rapidly dropped. This is reflected in the amount of energy stored in the PCM. On October 5 the spike around 16:00 caused a slight increase in stored energy. The average temperatures of the probes were fairly close, with the internal probes being the hottest on average, probably due to a combination of stratification and losses to

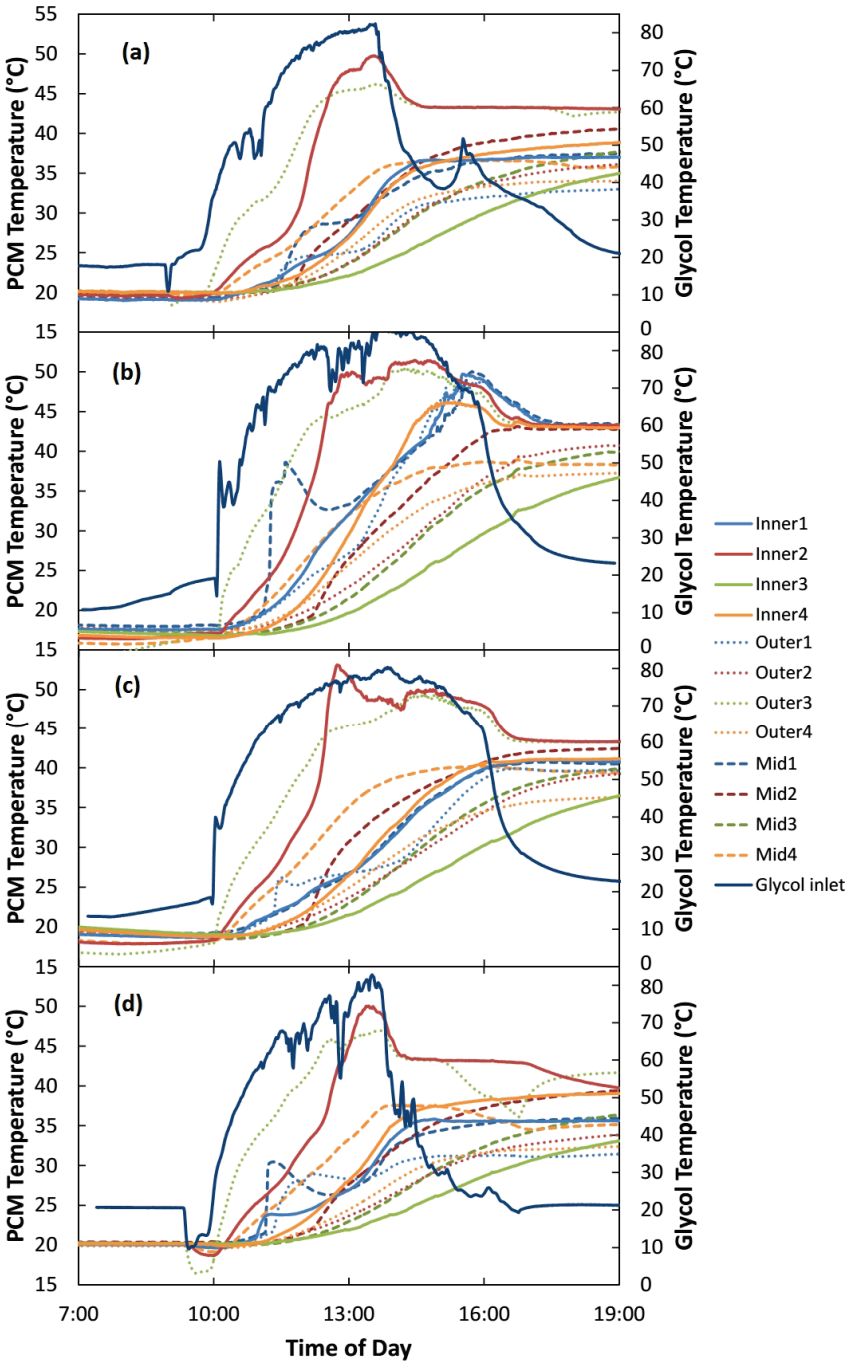

Figure 5.5: The PCM tank temperatures for October 5 (a), 10 (b), 19 (c), and 26 (d) of 2013. Time of day is Atlantic Daylight Time. PCM temperatures are on left axis and glycol temperature is on the right axis. For all days Outer3 and Inner2 are notable in that they rose in temperature much more quickly than the other probes. The rise in temperature of the PCM followed that of the heat transfer fluid, but with a time lag.

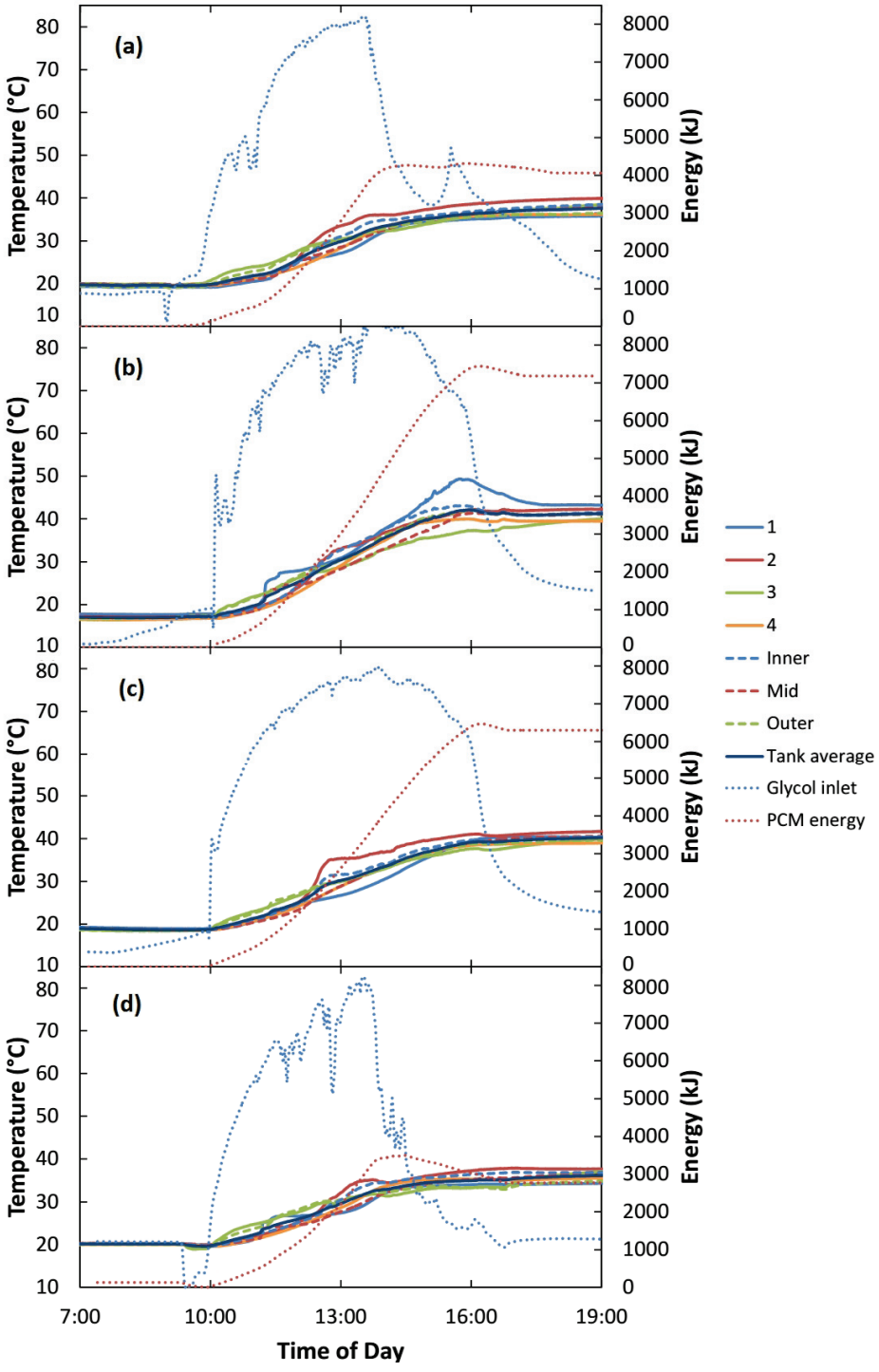

Figure 5.6: The average temperature measurements for October 5 (a), 10 (b), 19 (c), and 26 (d) of 2013. Values are averaged both laterally and by depth as well as a complete tank average. Times are in Atlantic Daylight Time. The energy the PCM absorbed from the heat transfer fluid is graphed on the right axis. To make all absorbed energy positive, the initial energy was set above zero.

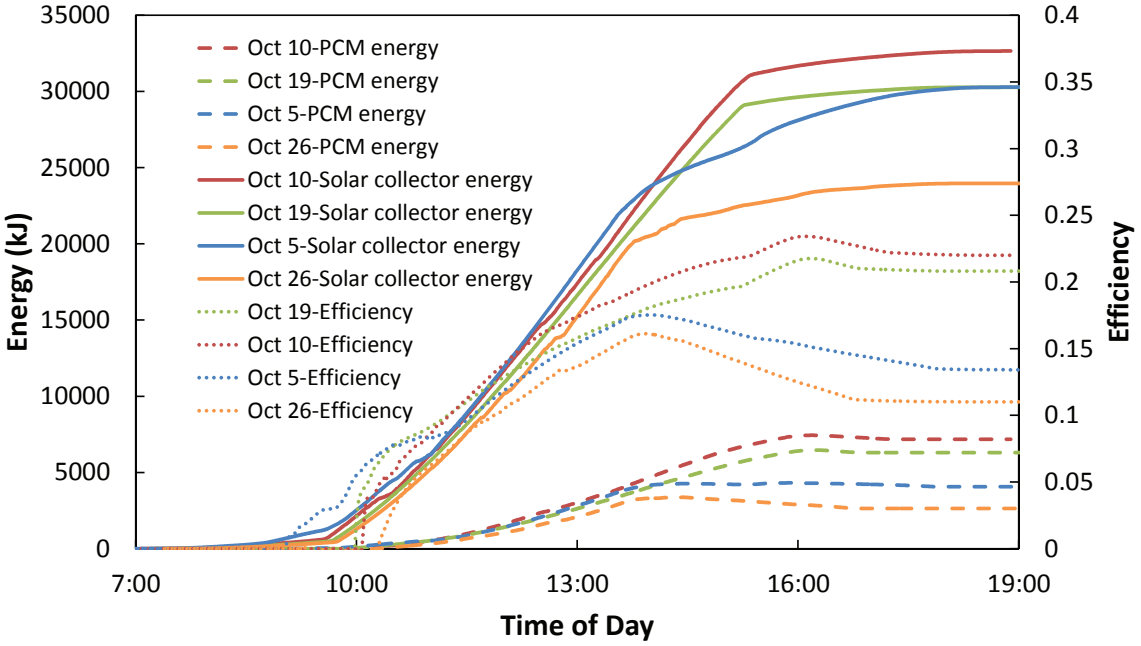

Figure 5.7: Energy stored or absorbed versus time for all four days (October, 5, 10, 19, and 26 2013). Several interesting details emerge in the combined graph. On days with longer sustained solar radiation and a more abrupt decrease in solar intensity, the system was more efficient and stored more energy.

the environment. On October 10, enough energy was absorbed to cause liquid to float to the top and for the average temperature of the "1" probes to be above the melting point of dodecanoic acid.

The energy absorbed by the collector and the PCM and efficiencies of the system are shown in Figure 5.7. As can be seen from that figure, between 3.4 and 7.4 MJ were absorbed in the course of a day. The linear trend in the energy absorbed versus time seen in Figure 5.7 is fairly typical for solar thermal systems using PCMs [71, 72]. The amount of energy absorbed was sufficient to commence melting of the dodecanoic acid, but not enough to melt all of the dodecanoic acid present. If the PCM started at 20 ℃ as in most of the tests, 3.32 MJ was expected to be stored as sensible heat in the solid phase (20 ℃ to 43 ℃), and the phase change at 43 ℃ was expected to store 11.0 MJ of energy. Therefore, during none of the days was enough energy absorbed to completely melt the dodecanoic acid. However, because the tank was not at equilibrium, some parts were able to become hotter than the melting temperature.

Nevertheless, operating the tank for between two and four of these days, without discharge of energy, would be sufficient to completely melt the contents of the tank. The equivalent to amount melted varied from 1% on October 26 2013 to as much as 35% on October 10 2013, based on the entire tank being at equilibrium. A study comparing how quickly this system absorbed energy with PCM or with water was performed by Joseph *et al.* [73] They determined that the low thermal conductivity of dodecanoic acid decreased the speed at which energy could be stored.

Additionally, the inlet and outlet temperatures for the glycol loop of the PCM tank are shown with the irradiance data in Figure 5.8. The strong dependence of these temperatures on irradiance can be seen.

Several parameters were assembled and assessed as can be seen in Figures 5.9 and 5.10. Some of the parameters are clearly correlated, and others are less so. The amount of energy absorbed by the PCM, the amount of energy absorbed by the collector, the efficiency and the percent melting of the PCM all correlated very well as can be seen in Figure 5.9. Efficiency here is gross system efficiency. It is defined as

$$\eta = \frac{E_{PCM}}{E_{collector}}, \tag{5.3}$$

where η is the system efficiency, E_{PCM} is the energy absorbed by the PCM, and $E_{collector}$ is the total power absorbed by the collector. This efficiency is not to be confused with the heat exchanger efficiency which is how effective the heat exchanger is at transferring heat from the heat transfer fluid to the PCM. Most of these correlations are fairly trivial because the more energy input into the system, the more energy the PCM would absorb. However, the reason why these energies would correlate with the efficiency is not as obvious. Essentially, when the collector absorbs more energy, the heat transfer fluid becomes significantly hotter, and the temperature differential between the heat transfer fluid and the PCM increases. A higher differential allows for better heat transfer and therefore a more efficient system. The discrepancy for the total energy the collector absorbed for the October 5 date (the second lowest efficiency in Figure 5.9) shows how this correlation can be thrown off. Some object, such as a cloud, occluded the solar panel on this day from about 14:00 to 15:30 as can be inferred from the data in Figures 5.6 and 5.8. During this time the pump was running and transferring some heat to the PCM. After a short amount of time

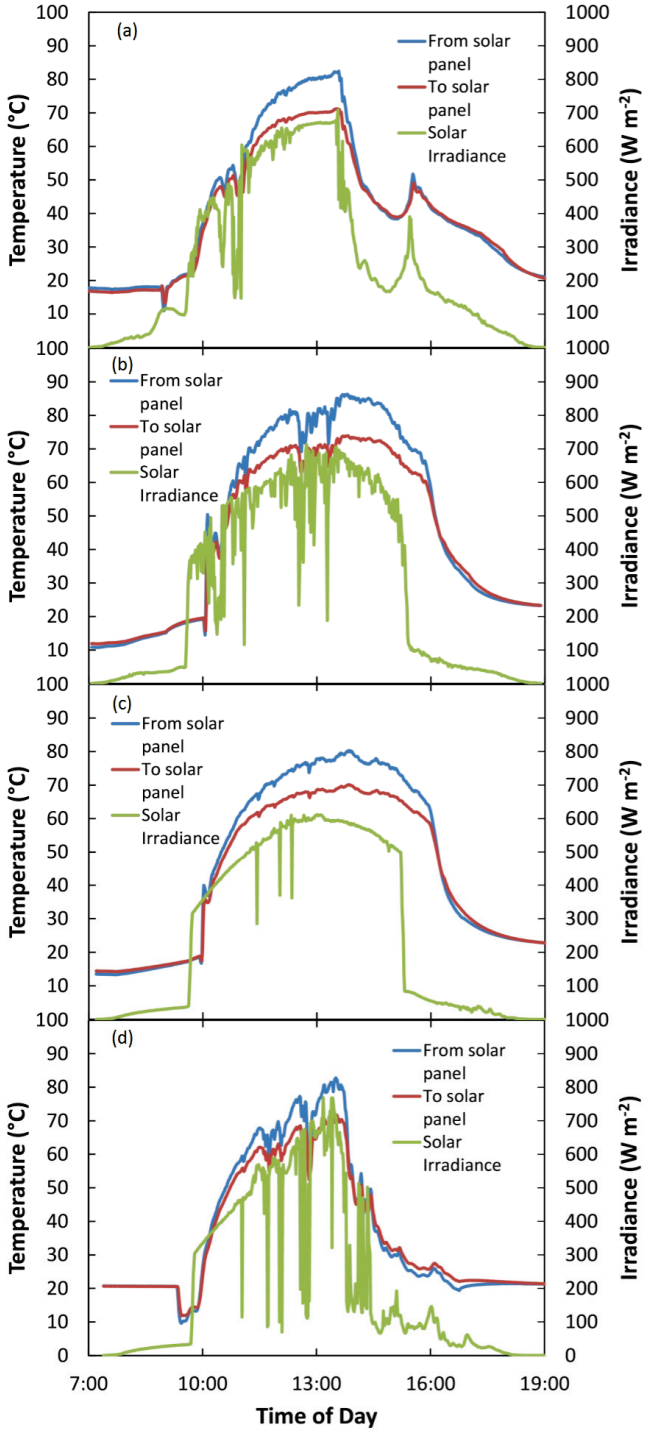

Figure 5.8: The inlet and outlet temperatures for the heat transfer fluid superimposed with the solar irradiance for October 5 (a), 10 (b), 19 (c), and 26 (d) of 2013. The fluid temperatures are strongly dependent on the intensity of the radiation.

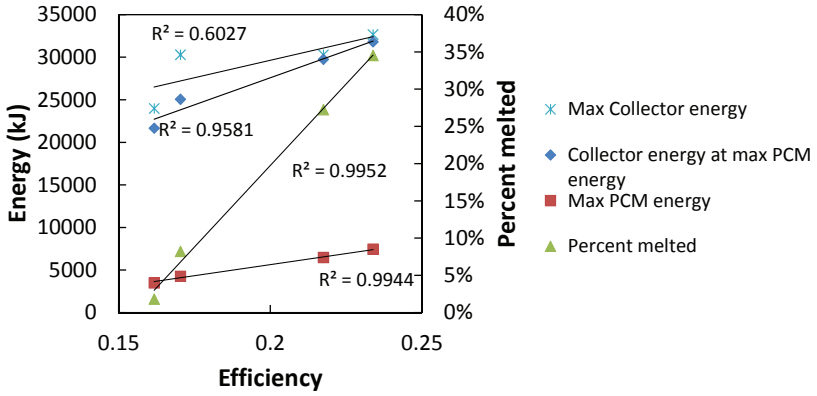

Figure 5.9: Parameters that correlated together well, graphed as a function of efficiency. Since these parameters all relate to how much energy was absorbed or stored, their correlation is reasonable.

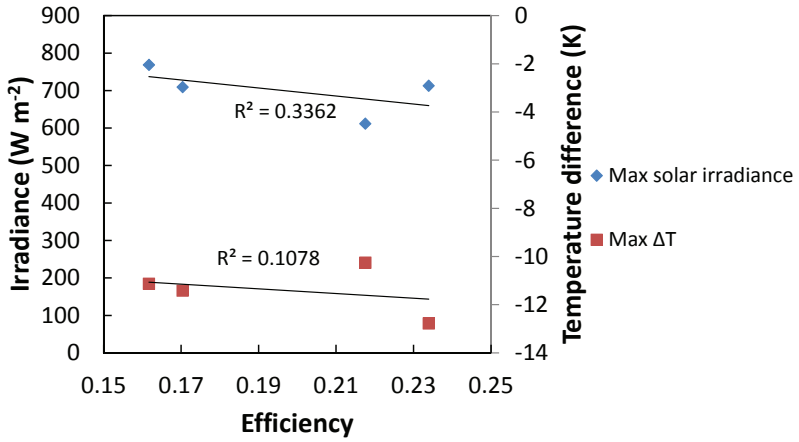

Figure 5.10: Parameters that do not correlate together well, graphed as a function of efficiency. These parameters may or may not be correlated to the other parameters based on the limited number of replicates. Additionally, these two parameters are more complicated than the others; for instance the maximum solar irradiance does not necessarily correlate with a high overall irradiance, *e.g.* a day when there were bright moments only at some points during the day.

the PCM was hotter than the heat transfer fluid, and thus the heat transfer fluid started to absorb heat from the PCM. As the light intensity increased again around 16:00, the temperature of the heat transfer fluid increased and a small amount of energy started going back into the system. This example shows the importance of a dedicated solar controller that monitors the temperature of the fluid and PCM and that starts or stops pumps as needed to prevent energy losses.

The efficiency and energy graphs in Figure 5.7 show that the measured days coincidentally fell into two broad categories. On October 10 and October 19 the panel had direct sunlight until it was shaded by the building, whereas on October 5 and October 26 the panel lost its direct sunlight. The amount of energy absorbed by the collector as seen in Figure 5.7 indicates this as well. For the October 10 and October 19 the curves abruptly change slope as there was no longer much light intensity after the panel became shaded. However, the heat transfer fluid was still hot so some energy continued to be transferred to the PCM, and the peak efficiency occurred about an hour after the direct sunlight stopped. The heat transfer fluid continued to transfer energy to the PCM after the sun went down because of the heat capacity of the heat transfer fluid. With the collector no longer absorbing energy, the efficiency increases, because of the way it is defined. On October 5 and October 26 the change of slope was more gradual, likely due to clouds blocking a significant proportion of the sunlight. Although there was still sunlight, it was not sufficient to warm the heat transfer fluid to as high a temperature, causing the efficiency to drop.

The major loss of this system is likely to be heat transfer away from the collector. By necessity the collector has a large area, and while this means it can efficiently absorb solar radiation, it also means it is vulnerable to heat loss. The other main risk to the system's efficiency is a situation in which the solar radiation is not of sufficient intensity to heat the heat transfer fluid above the temperature of the PCM. Comparing the system efficiency with other solar water heating systems it was slightly less efficient, with a commercial system being about 30 to 40% efficient [74]. Considering that this system is extremely unoptimized, the efficiency could be brought up with improvements to the heat exchanger design and better insulation.

5.5 Future Work

This system is a promising testbed for further research concerning the performance of actual solar thermal energy storage systems utilizing phase change materials. Several days of useful data were collected and analyzed. Since the system continuously records temperature, many additional days have data worth delving into. Information learned from this experiment can guide future experiments. Although this system is fairly robust, a few improvements are needed. Most important is a new pump or control system that can monitor thermal transfer fluid temperatures and tank temperatures and make decisions whether or not to turn on pumps to initiate heating or cooling. This system would insure that the PCM does not experience undesired losses to the outside.

The possibilities are plentiful for additional experiments. For example, various load regimes mimicking typical household use could be applied to assess the amount of heat that can be drawn from the PCM. A variety of heat exchangers, engineered to efficiently transfer heat in and out, could be inserted and compared against each other. These and other experiments show the value of this equipment as a fertile testbed for future research.

Chapter 6

Conclusions

This thesis has shown that phase change materials are effective heat storage materials in certain circumstances.

The phase change material must be well characterized and specifically designed for the application, and gaps in this knowledge have been identified in the present research. A list of PCMs and their physical characteristics in the form of a searchable spreadsheet was assembled to help with this task. Properties of $FeCl_3 \cdot 6H_2O$, $Mn(NO_3)_2 \cdot 4H_2O$, and $K_3PO_4 \cdot 7H_2O$ were measured and their practicable applicability as PCMs were assessed. $FeCl_3 \cdot 6H_2O$ was determined to have limited use, despite its high $\Delta_{fus}H$, as it supercools too strongly and its crystal growth rate is much too sluggish. $Mn(NO_3)_2 \cdot 4H_2O$ has a relatively low $\Delta_{fus}H$ but was found to experience little supercooling. Because salt hydrates that have small supercooling are rare, $Mn(NO_3)_2 \cdot 4H_2O$ was determined to have some potential as a PCM, at least enough to warrant further research. For $K_3PO_4 \cdot 7H_2O$ the $\Delta_{fus}H$ was measured and determined to be 132 $\pm$ 4 kJ kg^{-1} (288 $\pm$ 9 kJ L^{-1})* which is the first time $\Delta_{fus}H$ has been reported for this material. This $\Delta_{fus}H$ is relatively high on a volumetric basis, and as the crystal growth is quick and the anhydrous form is already a commodity product, $K_3PO_4 \cdot 7H_2O$ was determined to merit further study.

It is vital to do a life cycle assessment to quantify the utility of PCMs. The LCA presented in this thesis indicated that dodecanoic acid has good potential as a phase change material in solar thermal energy storage applications. A household solar thermal hot water system using dodecanoic acid was shown to save about 154 GJ and reduce CO_2 emissions by about 13.7 tonnes over 10 years. However, most dodecanoic acid comes from palm kernel oil (from the oil palm), mostly grown in Malaysia and Indonesia. Many of the new plantations are grown on land that was not cleared in an environmentally conscious way. Therefore, when responsibly using

*Based on solid density of 2.18 kg L^{-1}.

dodecanoic acid as a PCM, it is necessary to source it from certified environmentally friendly growers.

A solar thermal system utilizing dodecanoic acid was built and shown to effectively store energy. The amount of energy absorbed from the heat transfer fluid coming from the solar panel was quantified and analyzed. However, more work is needed to determine if it is a viable alternative to water as a storage medium for household solar thermal systems. The solar thermal system that was built will be useful for future studies.

This thesis presents work on many of the steps in the process to find materials that are excellent candidates for application as PCMs in solar thermal energy storage. A list of materials was assembled to isolate materials that have the required characteristics. Some of these materials were then researched further, to determine their utility as phase change materials. An LCA of a solar thermal energy storage system using dodecanoic acid was carried out. Finally, an actual system was then built and used to measure test conditions.

References

[1] Working group I contribution to the IPCC fifth assessment report climate change 2013: The physical science basis summary for policymakers `http://www.ipcc.ch/`.

[2] Canada's secondary energy use by sector, end-use and subsector Technical report Natural Resources Canada (2012) `http://data.gc.ca/`.

[3] Zalba, B., Marín, J. M., Cabeza, L. F., and Mehling, H. (2003) *Applied Thermal Engineering* **23(3)**, 251 – 283.

[4] Kosny, J., Petrie, T., Gawin, D., Childs, P., Desjarlais, A., and Christian, J. Thermal mass - energy savings potential in residential buildings, Buildings Technology Center, Oak Ridge National Laboratory `http://web.ornl.gov/sci/roofs+walls/research/detailed_papers/thermal/index.html` 2001.

[5] Belton, G. and Ajami, F. Thermochemistry of salt hydrates Technical Report NSF/RANN/SE/GI27976/TR/73/4 University of Pennsylvania (1973).

[6] Haynes, W., Lide, D., and Bruno, T. (2012) CRC Handbook of Chemistry and Physics, CRC Press, Cleveland, Ohio `http://hbcpnetbase.com/`.

[7] Hong, Y. and Xin-shi, G. (2000) *Solar Energy Materials and Solar Cells* **64(1)**, 37 – 44.

[8] Zhang, L.-J., Di, Y.-Y., Tan, Z.-C., and Dou, J.-M. (2012) *Solar Energy Materials and Solar Cells* **101(0)**, 79 – 86.

[9] Sharma, A., Tyagi, V., Chen, C., and Buddhi, D. (2009) *Renewable and Sustainable Energy Reviews* **13(2)**, 318 – 345.

[10] Abhat, A. (1983) *Solar Energy* **30(4)**, 313–332.

[11] Agyenim, F., Hewitt, N., Eames, P., and Smyth, M. (2010) *Renewable and Sustainable Energy Reviews* **14(2)**, 615 – 628.

[12] Tyagi, V. V. and Buddhi, D. (2007) *Renewable and Sustainable Energy Reviews* **11(6)**, 1146 – 1166.

[13] Lane, G. A. (1983) Solar Heat Storage: Background and Scientific Principles, CRC Press, Boca Baton, Florida.

[14] Lane, G. A. (1986) Solar heat storage: Latent Heat Materials, CRC Press, Boca Baton, Florida.

[15] Farrell, A. J., Norton, B., and Kennedy, D. M. (2006) *Journal of Materials Processing Technology* **175(13)**, 198 – 205.

[16] Telkes, M. (1952) *Industrial & Engineering Chemistry* **44(6)**, 1308–1310.

[17] Angell, C. A. and Tucker, J. C. (1974) *The Journal of Physical Chemistry* **78(3)**, 278–281.

[18] Gawron, K. and Schröder, J. (1977) *International Journal of Energy Research* **1(4)**, 351–363.

[19] Feldman, D., Shapiro, M., Banu, D., and Fuks, C. (1989) *Solar Energy Materials* **18(34)**, 201 – 216.

[20] Dall'Acqua, S., Fawer, M., Fritschi, R., and Allenspach, C. Life cycle inventories for the production of detergent ingredients. Technical Report 244 German Federal Environmental Agency and Oeko-Institut e.V. (1999) `www.zeolites.eu/downloads/LCIProdDet.pdf`.

[21] Sarı, A. and Kaygusuz, K. (2003) *Renewable Energy* **28(6)**, 939 – 948.

[22] Lane, G. A. and Glew, D. N. (1975) In Proceedings of the workshop on solar energy storage subsystems for the heating and cooling of buildings : 43 - 55.

[23] Mehling, H., Hiebler, S., and Gunther, E. (2010) *Applied Thermal Engineering* **30(17-18)**, 2652–2657.

[24] NIST Chemistry WebBook `http://webbook.nist.gov/chemistry`.

[25] Yaws, C. L. Yaws' handbook of thermodynamic and physical properties of chemical compounds `http://app.knovel.com/hotlink/toc/id:kpYHTPPCC4/yaws-handbook-thermodynamic`.

[26] Desgrosseilliers, L., Whitman, C. A., Groulx, D., and White, M. A. (2013) *Applied Thermal Engineering* **53(1)**, 37–41.

[27] Johnson, M. B. and White, M. A. Chapter 2: Thermal Methods, in Inorganic Materials: Multi Length-Scale Characterisation, Wiley (2014).

[28] Günther, E., Hiebler, S., Mehling, H., and Redlich, R. (2009) *International Journal of Thermophysics* **30(4)**, 1257–1269.

[29] Yinping, Z., Yi, J., and Yi, J. (1999) *Measurement Science and Technology* **10(3)**, 201.

[30] Lázaro, A., Günther, E., Mehling, H., Hiebler, S., Marín, J. M., and Zalba, B. (2006) *Measurement Science and Technology* **17(8)**, 2168.

[31] Kravvaritis, E. D., Antonopoulos, K. A., and Tzivanidis, C. (2010) *Measurement Science and Technology* **21(4)**, 045103.

[32] Hong, H., Kim, S. K., and Kim, Y.-S. (2004) *International Journal of Refrigeration* **27(4)**, 360–366.

[33] Marín, J. M., Zalba, B., Cabeza, L. F., and Mehling, H. (2003) *Measurement Science and Technology* **14(2)**, 184.

[34] Kravvaritis, E. D., Antonopoulos, K. A., and Tzivanidis, C. (2011) *Applied Energy* **88(12)**, 4459–4469.

[35] Moreno-Alvarez, L., Herrera, J. N., and Meneses, C. (2010) *Measurement Science and Technology* **21(12)**, 127001.

[36] Peck, J. H., Kim, J.-J., Kang, C., and Hong, H. (2006) *International Journal of Refrigeration* **29(7)**, 1225–1232.

[37] Nývlt, J. (1977) Solid-Liquid Phase Equilibria, Elsevier, New York.

[38] Wendrow, B. and Kobe, K. A. (1954) *Chemical Reviews* **54(6)**, 891–924.

[39] Weiner, M., Salminen, W., Larson, P., Barter, R., Kranetz, J., and Simon, G. (2001) *Food and Chemical Toxicology* **39(8)**, 759 – 786.

[40] Manufacturers, suppliers, exporters &; importers from the world's largest online B2B marketplace `www.alibaba.com`.

[41] Brandenburg, K. and Putz, H. Match! Software for phase identification from powder diffraction `http://www.crystalimpact.com/`.

[42] Hydromolysite mineral data `http://webmineral.com/data/Hydromolysite.shtml`.

[43] Manganese(II) nitrate hydrate 99.99% trace metals basis `http://www.sigmaaldrich.com/catalog/product/aldrich/203742`.

[44] Schmidt, J. H. (2010) *The International Journal of Life Cycle Assessment* **15(2)**, 183–197.

[45] Yee, K. F., Tan, K. T., Abdullah, A. Z., and Lee, K. T. (2009) *Applied Energy; Bio-fuels in Asia* **86, Supplement 1**, S189–S196.

[46] Castanheira, E. and Freire, F. (2011) In Sustainable Systems and Technology (ISSST), 2011 IEEE International Symposium on : 1 - 6.

[47] Lam, M. K., Lee, K. T., and Mohamed, A. R. (2009) *Biofuels, Bioproducts and Biorefining* **3(6)**, 601–612.

[48] Wei, P. C., May, C. Y., and Ngan, M. A. (2010) *Journal of Oil Palm Research* **22**, 927.

[49] U.S. Department of Agriculture, Agricultural Research Service. 2013. USDA National Nutrient Database for Standard Reference, Release 26 http://www.ars.usda.gov/ba/bhnrc/ndl.

[50] Ng, W. P. Q., Lam, H. L., Ng, F. Y., Kamal, M., and Lim, J. H. E. (2012) *Journal of Cleaner Production; Recent Cleaner Production Advances in Process Monitoring and Optimisation* **34(0)**, 57–65.

[51] Schmidt, J. H. and Weidema, B. (2008) *The International Journal of Life Cycle Assessment* **13(3)**, 235–239.

[52] Zulkifli, H., Halimah, M., Chan, K. W., Choo, Y. M., and Basri, W. M. (2010) *Journal of Oil Palm Research* **22**, 887.

[53] Muhamad, H., Hashim, Z., Subramaniam, V., Tan, Y. A., Wei, P. C., Let, C. C., and May, C. Y. (2010) *Journal of Oil Palm Research* **22**, 876.

[54] Subramaniam, V., May, C. Y., Muhamad, H., Hashim, Z., Tan, Y. A., and Wei, P. C. (2010) *Journal of Oil Palm Research* **22**, 895.

[55] Subramaniam, V., May, C. Y., Halimah, M., Zulkifli, J., Tan, Y. A., and Wei, P. C. (2010) *Journal of Oil Palm Research* **22**, 904.

[56] Gervajio, G. C. Fatty Acids and Derivatives from Coconut Oil, John Wiley & Sons, Inc (2005).

[57] Bhat, M. G., English, B. C., Turhollow, A. F., and Nyangito, H. O. Energy in synthetic fertilizers and pesticides: Revisited Technical Report ORNL/Sub/90-99732 Oak Ridge National Laboratory (1994) http://www.ntis.gov/search/product.aspx?abbr=DE94006309.

[58] Ashby, M. F. (2013) Materials and the Environment Eco-Informed Material Choice, Elsevier, 2nd edition.

[59] Fatty Acid Technology, volume **Technical brochure no. 274e/08.10/10**, Lurgi GmbH, Frankfurt am Main http://www.docstoc.com/docs/138201491/Fatty-Acid-Technology.

[60] Hang, Y., Qu, M., and Zhao, F. (2012) *Energy and Buildings* **45(0)**, 181–188.

[61] Myrans, K. Comparative energy and carbon assessment of three green technologies for a toronto roof, Master's thesis for University of Toronto, Department of Geography (2010) http://hdl.handle.net/1807/18905.

[62] Allen, S. R., Hammond, G. P., Harajli, H. A., McManus, M. C., and Winnett, A. B. (2010) *Energy* **35(3)**, 1351–1362.

[63] Masruroh, N. A., Li, B., and Kleme, J. (2006) *Renewable Energy* **31(4)**, 537–548.

[64] Thermo Dynamics Ltd. http://www.thermo-dynamics.com/.

[65] Greenhouse gas equivalencies calculator http://www.epa.gov/cleanenergy/energy-resources/calculator.html.

[66] Nova scotia power 2013 electricity rates http://www.nspower.ca/en/home/residential/billing/2013rates/default.aspx.

[67] Solar city program HRM http://www.halifax.ca/environment/SolarCity/.

[68] Hansen, S. (2007) *The International Journal of Life Cycle Assessment* **12(1)**, 50–58.

[69] Brown, E. and Jacobson, M. F. Cruel oil: How palm oil harms health, rainforest & wildlife (2005) Center for Science in the Public Interest http://www.cspinet.org/palm/PalmOilReport.pdf.

[70] Roundtable on sustainable palm oil http://www.rspo.org/.

[71] Ogoh, W. and Groulx, D. (2012) *Heat and Mass Transfer* **48(3)**, 439–449.

[72] Garg, H., Mullick, S., and Bhargava, A. K. (1985) Solar Thermal Energy Storage, D. Reidel Publishing Company, Dordrecht, Holland.

[73] Joseph, A., Kabbara, M., Groulx, D., Allred, P., and White, M. A. (2014) In International Conference on Clean Energy 2014 : Submitted Paper.

[74] CLEAN ENERGY PROJECT ANALYSIS: RETSCREEN ENGINEERING & CASES TEXTBOOK chapter SOLAR WATER HEATING PROJECT ANALYSIS Natural Resources Canada (2004).